Thallium concentration and thallium isotope composition of lateritic terrains

Howarth, S.[1,2*], Prytulak, J.[1, 3], Little, S. H.[1], Hammond, S. J.[4], Widdowson, M.[5]

[1]Department of Earth Science and Engineering, Imperial College London, SW7 2AZ, UK

[2]National Oceanography Centre, School of Ocean and Earth Science, University of Southampton, SO14 3ZH, UK. S.A.Howarth@soton.ac.uk

[3]Department of Earth Sciences, University of Durham, DH1 3LE, UK

[4]School of Environment, Earth and Ecosystem Sciences, The Open University, Walton Hall, Milton Keynes, MK7 6AA, UK

[5]School of Environmental Science, University of Hull, Cottingham Road, Hull, HU6 7RX, UK

ABSTRACT

Continental weathering plays a key role in modifying the geochemical budget of terrestrial reservoirs. Laterites are the products of extreme sub-aerial continental weathering. This study presents the first investigation of thallium (Tl) abundances and stable isotopic compositions of lateritic terrains. Two laterite profiles from India of differing protolith and age are studied. Thallium concentrations range between 7 – 244 ng/g for a basalt-based lateritic profile and 37 – 652 ng/g within a greywacke lateritic profile. The average Tl stable isotope composition of the two profiles is similar to many typical igneous materials, however, the intense tropical weathering causes a small but resolvable fractionation of Tl stable isotopes towards heavy values in the residual soils. The profiles are dominated by significant positive isotope excursions (reported as ε^{205}Tl relative to standard NBS997) of + 3.5 ± 0.5 2sd and + 6.2 ± 0.5 2sd at the inferred palaeowater tables within both laterite profiles. These signatures likely reflect combined changes in redox state and mineralogy. Extensive mineral dissolution under through-flowing fluids alongside the formation of new phases such as phyllosilicates and Mn- and Fe- oxides and hydroxides likely account for some of the Tl mobilisation, sorption and coprecipitation. In the case of laterites, the formation of the new phases and role of surface sorption likely contribute to stable Tl isotope fractionation. The identification of strong isotope excursions at inferred palaeowater tables encourages future research to determine specific mineral phases that may drive significant fractionation of Tl stable isotopes. This study showcases the magnitude of natural variation possible in terrestrial soils. Such information is key to the nascent applications of Tl isotope compositions as tracers of anthropogenic pollution.

Keywords: *Laterites, Thallium Isotopes, Ferromanganese Minerals, Birnessite*

41 **1. INTRODUCTION**

42 The weathering of continental landmasses is one of the major modification processes
43 operating on the surface of the Earth. It plays a significant role in the geochemical cycling of
44 elements, from local to global scales. The effects of oxidative weathering on elemental
45 mobility are also an important consideration for environmental impact studies. Improvements
46 in analytical techniques in recent decades have enabled stable isotope analysis for elements
47 spanning the periodic table (e.g., Bullen, 2012, 2014; Wiederhold, 2015; Teng et al., 2017).
48 Such stable isotope investigations (e.g., Cr, Li, Fe, Cu, Ni) are increasingly providing insight
49 both into continental weathering processes (e.g., Huh et al., 1998; Gall et al., 2013; Berger
50 and Frei, 2014; Wiederhold, 2015) and the formation of laterites specifically (e.g., Kisakürek
51 et al., 2004; Poitrasson et al., 2008; Liu et al., 2014). One element and novel isotope system
52 whose weathering behaviour remains relatively unexplored is that of thallium (Tl).

53 The distribution and behaviour of Tl in terrestrial reservoirs is partly controlled by
54 similarities of its relatively large ionic radius (Tl^+ = 1.50 Å) to the alkali metals K^+, Rb^+ and
55 Cs^+ (Shaw, 1952; Heinrichs et al., 1980). This has been used to explain the observed
56 differences in Tl concentration between continental crust (~0.5 μg/g) and mantle (~0.003
57 μg/g) (Fig. 1) due to its incompatible behaviour during mantle melting (Shaw, 1952;
58 Heinrichs et al., 1980; Nielsen et al., 2006b; Nielsen et al., 2017a; Prytulak et al., 2017). Ionic
59 charge is also likely to factor into the behaviour of Tl, given its existence in both monovalent
60 and trivalent valence states (Nielsen et al., 2017a). Within low temperature environments,
61 studies have focused largely on the most Tl-enriched reservoirs, hence the comparative
62 wealth of work on ferromanganese (FeMn) crusts and nodules in the marine realm (e.g.
63 Rehkämper et al., 2002; Nielsen et al., 2009, 2011, 2013; Peacock and Moon, 2012).
64 Ferromanganese crusts have some of the highest natural Tl concentrations determined thus
65 far, between 30 – 200 μg/g (Fig. 1) and as such are a key reservoir in the global Tl cycle.

Thallium abundances within soils are comparatively low, normally ranging from 0.01 – 1 µg/g for uncontaminated soils (Kazantis, 2000; Xiao et al., 2004). Some soils have shown naturally elevated concentrations >5 µg/g. These tend to be associated with K-rich igneous rocks, where similar ionic radii allow for substitution of K^+ or Rb^+ with Tl^+, or soils occurring proximal to sulfide deposits (Xiao et al., 2004; Pavlíčková, 2006). Finally, high Tl concentrations proximal to industrial hubs has focused recent environmental research on tracking anthropogenic Tl pollution and contamination. Surface soil Tl concentrations have been shown to depend not only on substrate lithology but also on the presence of anthropogenic Tl contamination, for example from cement plants (e.g. Jacobson et al., 2005; Pavlíčková, 2006; Vaněk et al., 2009; Kersten et al., 2014; Vaněk et al., 2016; Vaněk et al., 2018). Studies of heavily contaminated soils (hundreds to thousands of µg/g Tl) have observed Tl associations largely with residual silicates and secondary illite-clays. Furthermore, in soils with lower Tl concentrations (few tens of µg/g Tl) the Tl adsorption appears dominated by Mn-oxides, with negligible adsorption onto Fe(III) oxides such as goethite (Vaněk et al., 2009; Vaněk et al., 2011; Voegelin et al., 2015; Vaněk et al, 2016).

Thallium stable isotope studies in low temperature environments have highlighted surprisingly large isotope fractionations. Despite the small relative mass difference between the two Tl isotopes (^{203}Tl and ^{205}Tl) of <1%, Tl displays large natural isotope variations in excess of 35 epsilon units (corresponding to 3.5‰ in the δ-notation, as used in other isotope systems) in low temperature environments. Isotope variations are reported relative to the NIST 997 Tl standard as ε^{205}Tl, which is defined as:

$$\varepsilon^{205}\mathrm{Tl} = \left(\left(\frac{\left({}^{205}Tl/{}^{203}Tl\right)_{sample}}{\left({}^{205}Tl/{}^{203}Tl\right)_{NIST\ 997}} \right) \text{-}1 \right) \times 10,000$$

By far the largest Tl isotope fractionations have been observed within marine reservoirs and extensive work has been carried out on FeMn crusts and altered oceanic crust, which

90 display large positive and negative ε^{205}Tl signatures, respectively (Fig. 1; see review in
91 Nielsen et al. 2017a). In FeMn crusts, coupled sorption and redox effects onto specific Mn-
92 oxides has been shown to cause Tl stable isotope fractionation (Peacock et al., 2009; Peacock
93 and Moon, 2012; Nielsen et al., 2013). Within terrestrial environments a smaller range of
94 ε^{205}Tl have been recognised. Similar Tl stable isotope values for upper continental crust and
95 riverine detrital particulates (average ε^{205}Tl of −2.0 and −2.5 respectively) have been used to
96 imply negligible Tl fractionation during weathering processes, however the direct effect of
97 weathering is yet to be studied extensively (Nielsen et al., 2005). Investigations of soils have
98 focussed on the use of Tl stable isotope compositions as tracers of industrial processes, such
99 as cement production and coal burning. This application relies on the existence and
100 preservation of an 'anthropogenic' Tl stable isotope signature. However, the potential
101 secondary Tl stable isotope effects from lithospheric and pedospheric processes remain
102 poorly defined and require further investigation to better aid reliable tracing of industrial Tl
103 emissions (Kersten et al., 2014; Voegelin et al., 2015; Vaněk et al., 2016). Potential sources
104 of fractionation include riverine transport processes and continental weathering: the latter
105 providing the impetus for the current study. Since lateritic profiles represent some of the most
106 extreme enrichment and depletion behaviours that occur naturally in rock substrates as well
107 as systematic mineralogical changes, they provide a natural laboratory to investigate Tl
108 behaviour during weathering.
109 Here we provide the first examination of Tl and stable Tl isotope variations resulting
110 from intensive oxidative weathering processes through the investigation of well-
111 characterized, mature, deep weathering profiles of tropical lateritic terrains. We aim to
112 determine the magnitude of Tl elemental and isotope variation and its most likely cause(s).
113 Given the extent of laterites through geological time, covering ~30% of continental surface
114 area (Tardy, 1997; Dequincy et al., 2002) and with protracted formation periods,

115 understanding the behaviour of Tl in extensively weathered terrains could provide important
116 insights into the little-explored behaviour of Tl in surface environments. Furthermore, our
117 work also provides a baseline for nascent industrial anthropogenic pollution applications.
118
119 **2. METHODS**
120 *2.1. Sample Suites*
121 Two well-characterised, lateritic profiles from India of differing substrate and ages were
122 chosen: the basaltic-based Bidar and greywacke-based Merces Quarry sequences
123 (Widdowson, 2007). The spatial association of the two profiles restricts the effects of major
124 climatic variations, and their geographic situation minimizes potential differences in exotic
125 inputs (Fig. 2; Babechuk et al., 2015). The two profiles are extensively characterised with
126 respect to elemental composition, mineralogy and degrees of lateritization (Mason, 1999;
127 Widdowson and Gunnell, 1999a, 1999b; Borger and Widdowson, 2001; Kisakürek et al.,
128 2004; Wimpenny et al., 2007; Widdowson, 2009; Babechuk et al., 2014, 2015).
129 The Bidar Profile (hereafter "BB") is a lateritic sequence through the Deccan flood
130 basalts, near Bidar, north-eastern Karnataka State, Central India (17°54'43'' N,
131 77°32'38''E). This 50 m deep weathering profile is capped by a thick, indurated laterite
132 which is likely to have developed between ca. 65 – 55 Ma (Widdowson and Gunnell, 1999a,
133 1999b) directly upon the Ambenali Formation (Fm) of the Late Cretaceous Deccan basalt
134 succession (Widdowson, 1997; Babechuk et al., 2015). This formation is part of the Deccan
135 Traps, a Continental Flood Basalt Province (CFBP) erupted over ~4 Ma period at 67 - 63 Ma
136 and consisting of multiple tholeiitic flow bodies, of which the Ambenali Fm is the most
137 extensive (Jay and Widdowson, 2008).
138 The Merces Quarry (hereafter "SQ") example is a 35 m weathering profile developed
139 upon a metagreywacke and forming part of the Panjim-Merces Plateaux in Goa, western

India (15°28.46’ N, 73°52.33’) (Widdowson, 2009). It lies within the Konkan-Kanara lowlands, and formed as an extensive belt of laterite during the mid-Neogene (Miocene) at ca. 10 – 20 Ma (Schmidt et al., 1983). The protolith is a weakly metamorphosed early Proterozoic greywacke of the Goa Group (Sanvordem Fm) of the Dharwar Supergroup. This complex comprises part of the extensive basement lithologies that underlie the Deccan CFBP and which become exposed in the south of ca. 16°N.

Both profiles follow the idealised laterite profile with an unaltered bedrock (i.e., protolith) at its base that is overlain by a progression into saprock, then saprolite, in which the primary texture of the rock is preserved, and then into increasingly altered zones above (Fig. 3; e.g. Martini and Chesworth, 1992; Widdowson, 2007). The saprolite zone often contains unaltered corestones within a soft saprolite matrix. Lateritization intensity increases up-profile, through the mottled zone and carapace (i.e., non-indurated levels dominated by oxyhydroxides of Fe and Al), with any remaining primary textures obscured by iron-rich segregations (i.e., mottled zone) and an increasingly open porosity eventually characterised by tubular (i.e., vermiform) textures. Both are capped by a highly indurated, resistant duricrust. The weathering of basaltic and related substrates typically involves the alteration of a mafic mineral assemblage firstly to phyllosilicates, followed by kaolinization and desilicification (Nesbitt and Young, 1989); the detail of this pattern can vary in those profiles developed on more felsic, or sedimentary protoliths (e.g. Fedo et al., 1995).

Here, we focus on those samples most representative of the mineralogical and textural changes within two contrasting laterite sequences, of different substrate types and ages (Fig. 3; Mason, 1999; Kisakürek et al., 2004; Babechuk et al., 2014).

Within the SQ profile, SQ2 represents the unweathered greywacke horizon. Sample SQ1 represents a small-scale mafic dyke (Widdowson, 2009). Samples SQ3 – SQ4, lie within the saprock zone. Samples SQ5 and SQ7 – SQ9, ~ above 22.5m, lie within the kaolinization field

and correspond to Si-depletion and Fe-enrichment, transitioning from upper saprolite and plasmic zone into the mottled zone with Fe-rich segregation. Samples SQ10 and SQ13 – SQ14 are strongly lateritized and correspond to the carapace and indurated duricrust. Samples SQ12 and above mark the progression towards secondary Fe-dominated minerals as more Si and Al is lost from the neo-formed kaolinite. Within the BB profile, samples BB1 and BB2 represent the unaltered Deccan basalt and proximal saprock within Zone I that display similar chemical compositions. Samples BB3 and BB4 show mottled textures within the saprock of Zone II. BB7 and BB8 correspond to weak and moderate lateritization and the uppermost BB9 represents the indurated duricrust (Fig. 3). Extensive work carried out by Widdowson (2007) detailed the variation in major elemental composition through both the BB and SQ profiles. In both profiles, the more mobile elements (e.g. Ca, Mg, K) are lost from the saprolite zones (Zone II, Fig. 3). Above the saprolite zones an increase in Fe concentration is observed alongside a decrease in Si due to the breakdown of the protolith silicates. The small increase of SiO_2 in SQ6 is attributed to its proximity to a quartz vein within the profile, highlighting the greater variability in the SQ protolith. The uppermost sections of both profiles, corresponding to the iron-rich duricrust (Zone IV), show the expected enrichments in Fe_2O_3 and corresponding depletion in SiO_2. In both profiles, there are horizons that do not follow this sequence of laterite development, BB5 and BB6 in the Bidar laterite and SQ10 and SQ11 in the SQ laterite (Zone III, Fig. 3). Concentrations of Fe_2O_3 and trace elements, alongside Os and Li isotopic data, have shown that these enrichments can be attributed to the existence of palaeowater tables, which has allowed for the allochthonous input of Fe via groundwater fluxes (Kisakürek et al., 2004; Wimpenny et al., 2006).

2.2. Sample Preparation

189 The BB and SQ samples used, from the Bidar and Merces Quarry respectively, were
190 collected by previous studies and were chosen as representative of key horizons that marked
191 changes in mineralogy and texture (Mason, 1999; Wimpenny et al., 2007). Bulk samples of 1
192 – 3 kg of each horizon were originally collected from multiple representative outcrops to
193 reduce the effect of local heterogeneities within horizons (Kisakürek et al., 2004). Samples
194 for the BB profile were powdered in a tungsten carbide mill, whereas samples for the SQ
195 profile were prepared in an agate mill to minimize potential contamination. It should be noted
196 that preparation in tungsten carbide versus agate is not anticipated to affect Tl concentration
197 or isotope ratios.
198
199 *2.3. Major and trace elements*
200 Major element data for both the BB and SQ sequences and supplementary trace element
201 data for the BB profile are from Babechuk et al. (2014) and Widdowson (2007). We report
202 new high precision trace element determinations, including Tl, for both the BB and SQ
203 sequences.
204 Trace element analysis was undertaken at the Open University, UK, with an Agilent
205 8800 ICP-QQQ ('triple-quad' inductively coupled plasma mass spectrometer). Sample
206 digestion was performed at the Mass Spectrometry and Geochemistry Labs at Imperial
207 College London (MAGIC). All acids employed in chemical digestions and separations were
208 distilled in either quartz or Teflon sub-boiling distillation systems and all Savillex Teflon was
209 acid cleaned. De-ionized, 18 MΩ-grade water from a Millipore system-was used for rinsing
210 and dilution. Approximately 50 mg of sample powder was dissolved in sealed Teflon vials
211 with a 3:1 mixture of concentrated HF: HNO_3. The solutions were ultra-sonicated for 25
212 minutes and heated at 160 °C on a hot plate for at least 24 hours. They were then evaporated
213 to near dryness and re-dissolved in 2 ml of 6 M HCl at 120 °C for at least 24 hours. The

214 solutions were then evaporated to complete dryness at 120 °C and re-dissolved in ~1 ml
215 concentrated HNO_3 and evaporated at 180 °C. The last re-dissolution and evaporation step
216 was repeated at least three times until the samples turned brownish or brown, indicating the
217 destruction of fluorides from initial HF dissolution. Finally, an appropriate volume of 2%
218 HNO_3 was added to achieve a 1000-fold sample dilution.
219 Samples were aspirated into the ICP-QQQ using a quartz microflow nebuliser, with an
220 uptake rate of 0.5 ml per minute, and count rates in the order of $1 – 5 \times 10^7$ cps/ppm.
221 Analyses were performed in two different collision/reaction cell modes (no gas and He).
222 Oxide levels (measured as CeO/Ce) were kept low, at 1% in no gas, and 0.5% in He collision
223 mode, and doubly charged species (Ce++/Ce+) at 1.6% in no gas, and 1.2% in He collision
224 mode. Analyses were standardized against five reference materials (digested at both the Open
225 University and Imperial College London) that were measured at the beginning of each
226 analytical run. The reference materials were selected on the basis of their similarity to the
227 samples analysed, and include BIR-1, W-2, DNC-1, BHVO-2 and AGV-1. An internal
228 standard solution (containing Be, Rh, In, Tm, Re, and Bi) was added to samples and run on-
229 line throughout all analyses and used to correct for instrumental drift. Drift was further
230 monitored with a measurement block consisting of USGS reference material BIR-1 (separate
231 digest to that used in the standardization), a 2% HNO_3 blank, and a repeated unknown sample
232 (SQ8) performed every five unknown measurements (see Supplementary Sheet 3). After
233 correction for the blank values, instrumental drift and dilution weights, replicate
234 measurement of monitoring standards yielded a precision of <2% RSD for Tl (see
235 Supplementary Sheet 3 and Sheet 4 for trace elemental precision data). Thallium
236 concentrations determined by ICP-MS (QQQ) are in agreement with estimated values
237 obtained during MC-ICPMS isotope measurements (see Electronic Annex). We employ ICP-
238 MS (QQQ) for Tl data measured in this study in all subsequent figures, due to its superior

239 precision and accuracy compared to the greater error associated with concentration
240 determination by beam intensity matching during MC-ICPMS isotope measurements.
241
242 *2.4. Determination of Tl stable isotope composition*
243 Separation of Tl from sample matrices was carried out in the MAGIC Laboratories at
244 Imperial College London following established two-stage ion exchange chromatography
245 protocols (Rehkämper and Halliday, 1999; Nielsen et al., 2004; Prytulak et al., 2013).
246 Thallium stable isotope compositions were determined using a Nu-Plasma HR MC-
247 ICPMS, equipped with an ARIDUS II introduction system. Thallium fractions were diluted
248 to concentrations between 2 and 5 ppb and doped with NIST SRM 981 Pb for a Pb/Tl ratio of
249 ~4 in order to correct for instrumental mass fractionation. Thallium isotopes were measured
250 using sample-standard bracketing techniques with NIST SRM 997 Tl (Rehkämper and
251 Halliday, 1999). As the column chemistry method used provides quantitative Tl yields, with
252 Rehkämper and Halliday (1999) confirming routine Tl elutions of >99.5% in the applied
253 anion-exchange procedure, Tl concentrations can be estimated to a precision of ~10-15%
254 through monitoring ^{205}Tl intensities using a MC-ICPMS (Rehkämper and Halliday, 1999;
255 Nielsen et al., 2004; Nielsen et al., 2005; Prytulak et al. 2013). Multiple reference materials
256 with known ε^{205}Tl values were run for data quality control. United States Geological Survey
257 (USGS) reference material AGV-2 and/or BCR-2 were processed and measured with every
258 batch of unknown samples. We also present the first Tl isotope measurements of VL2, a
259 laterite standard from Venezuela developed upon a doleritic protolith (Schorin and
260 LaBrecque, 1983; LaBrecque and Schorin, 1987). Thallium concentrations and stable isotope
261 composition of the samples and standards are given in Table 1 and 2. The Tl isotope
262 composition of USGS reference materials AGV-2 and BCR-2 measured over the course of
263 this study agree with literature values (Table 2). Repeat analyses of a Sigma Aldrich Tl

solution standard has shown a long-term measurement reproducibility of $\varepsilon^{205}Tl = -0.79 \pm 0.35$ (compiled by Nielsen et al., 2017a). This study determined the Sigma Aldrich standard as $\varepsilon^{205}Tl = -0.61 \pm 0.36$ (n = 33), in agreement with this reproducibility. Replicate digestions of most samples measured show an external 2sd reproducibility of about ± 0.5 $\varepsilon^{205}Tl$. A standard error of ± 0.5 $\varepsilon^{205}Tl$ is applied to all samples except those whereby the calculated 2sd between replicates exceeded this value. This includes sample BB5, with $\varepsilon^{205}Tl = +6.2 \pm 1.5$ 2sd (n = 4), encompassing 3 separate dissolutions. Table 1 shows that there is a discrepancy between the $\varepsilon^{205}Tl$ measured for each separate dissolution, but within the second dissolution the results are self-consistent, with an average of $\varepsilon^{205}Tl = +6.2 \pm 0.7$ (2sd, n = 2). Thus, we attribute the larger external reproducibility of this sample to powder heterogeneity, potentially generated during field sampling of this complex horizon. Total procedural blanks were <20 pg Tl, negligible relative to the total processed Tl (>24 ng).

3. RESULTS

3.1. Thallium and other trace elements

Thallium concentrations and trace element determinations are shown in Tables 1 and 3.

The SQ profile reveals Tl concentrations ranging from 37 – 652 ng/g (Table 1, Fig. 4a), displaying an overall depletion in Tl when compared to average values for the upper continental crustal of ~750 ng/g (Taylor and McLennan, 1985). The overall Tl concentration profile with depth in SQ is highly variable. The median concentration is 132 ng/g but the profile is dominated by high concentration spikes, with four samples exceeding the upper quartile value of 414 ng/g. Two key positive excursions in concentration occur at 22.5 m for SQ5 (652 ng/g) and 7.5 m for SQ11(544 ng/g). The lowest Tl concentration, of 37 ng/g, is at 8.5 m (SQ10).

Concentrations of the four samples measured using ICP-QQQ for the BB profile range from 7 – 244 ng/g (Tables 1 and 2). Thallium concentrations for the full depth profile were carried out by Babechuk et al. (2014), and show a comparable range between 3 – 272 ng/g. The Bidar profile shows an increase in measured concentrations up-section, from 7 ng/g at 26 m (BB3) to 39 ng/g at 5 m (BB8), with the highest concentration (244 ng/g) found at 6.0 m (BB7) (Fig. 4b).

The trace element concentrations within the SQ and BB profiles show similarly large variance (Table 3 and Fig. 5). Given predicted similar behaviours between Tl and elements that form species with similar ionic radii, the concentration profiles of the alkali elements can be compared. Within the SQ profile, the trace alkali elements (Cs, Li and Rb) share almost identical patterns of depletion and enrichment relative to unweathered protolith concentrations (Fig. 5a). These match the patterns of Tl through most of the profile but display markedly different behaviour for sample SQ11. Here the alkali elements do not display the extreme enrichment observed for Tl. Similarly, the trace alkaline earths (Sr and Ba) show varying concentrations relative to the Tl concentration pattern. Enrichments and depletion patterns above protolith values are well matched by Ba but Sr displays much smaller variance and depletion within all weathered samples. Within the BB profile the alkali elements also show similar patterns of enrichment and depletion relative to each other but behaviour compared to Tl deviates at BB8 and BB7 (Fig. 5b). At these horizons, the alkali elements are enriched in BB8 and depleted in BB7, which opposes the trend for Tl in both samples. For the trace alkaline earths Ba and Sr enrichments relative to the protolith are decoupled through the profile, with Ba displaying similar trends to Tl.

3.2. Thallium stable isotope variation in laterite profiles

312 The SQ sequence shows a large range in ε^{205}Tl from – 2.4 to + 3.5, which is variable
313 throughout the profile but generally shows a slight increase in ε^{205}Tl up-profile, with the
314 exception of a prominent positive excursion of ε^{205}Tl = + 3.5 at SQ11 (Fig. 4b).
315 The lightest ε^{205}Tl value occurs at 25.5 m for SQ4 and the heaviest occurs at 7.5 m for
316 SQ11 (Fig. 4b). There is a slight general increase in The BB sequence ε^{205}Tl values range
317 from – 0.5 to + 6.2. The lightest ε^{205}Tl is BB8 at 5 m (Fig. 4b). Trends within the profile are
318 less well defined due to fewer data points, but at 13 m the outlying and distinctive feature is
319 an excursive heavy ε^{205}Tl = + 6.2 for BB5. The profile average for all samples analysed is
320 ε^{205}Tl = + 2.0 ± 3.7 (1sd, n = 3). Low Tl concentrations (e.g., BB1 ~3 ppb; Babechuk et al.,
321 2014) require in excess of 1 g of sample for repeat Tl isotopic measurement, of which there
322 was insufficient characterised material remaining. However, unweathered basalt is assumed
323 to have Tl content comparable to mid-ocean ridge basalts (MORBs) (Nielsen et al., 2006a),
324 hence a value of ε^{205}Tl ~ – 2.0 ± 1 is assumed for the protolith (BB1) (e.g. Fig 4). When this
325 assumed value of ε^{205}Tl is used to approximate BB1 the average for the profile is ε^{205}Tl = +
326 1.0 ± 7.2 (2sd, n = 4). For the BB sequence a correlation between Tl concentrations and
327 ε^{205}Tl cannot confidently be drawn due to the small dataset but the excursive nature of BB5 is
328 clear (Fig. 6). The VL2 laterite standard measured shows a heavy ε^{205}Tl = + 2.1 ± 0.5 which
329 is closely matched to the average Tl isotopic composition of the BB profile.
330

331 **4. DISCUSSION**

332 Both the basaltic BB and greywacke-based SQ sequences show variable depth profiles
333 with respect to both Tl concentrations and stable isotope signatures (Fig. 4a and 4b). *A priori*
334 these variations could be considered the result of two natural factors. Firstly, processes
335 internal to the laterite profile, which could drive redistribution of Tl and/or significant stable
336 isotope fractionation. Secondly, external fluxes of Tl to and from the laterite profiles.

337 In order to quantify the overall addition and loss of elements in weathering profiles,
338 relative to the unaltered protolith levels, we calculate the τ-parameter following Chadwick et
339 al. (1990). The τ-parameter describes the proportion of a selected element gained or lost at a
340 chosen horizon within a weathering profile, relative to an immobile index element. The least
341 mobile element identified for both profiles was Zr, because it displays the smallest variation
342 relative to protolith concentrations (Widdowson and Cox, 1996). The τ-parameter is
343 calculated as follows:

344 $$\tau_{i/Zr} = \left[\frac{(C_i/C_{Zr})_h}{(C_i/C_{Zr})_p}\right] - 1$$

345 where C is the concentration, h represents the horizon of interest and p represents the
346 unaltered protolith values (samples BB1 and SQ2). τ-values are shown in Table 4. Values > 0
347 indicate enrichment of element of interest *i* and values < 0 indicate loss of *i* relative to the
348 unweathered substrate. When summed throughout the profile the total τ-value can give an
349 indication of net gain or loss of element *i* to the profile versus internal mobilization and
350 vertical transport.

351 The extent of weathering through the profiles also needs to be quantified in order to
352 investigate the role of weathering and chemical alteration on Tl concentration and stable
353 isotope systematics. The most commonly applied indices of chemical alteration used are the
354 Chemical Index of Alteration (CIA) and the Mafic Index of Alteration (MIA). Both employ
355 bulk major elemental molar ratios but do not include the proportion of SiO_2 in their
356 calculations and insufficiently capture the more extreme, late-stage weathering and
357 desilicification processes which occur during lateritization (Babechuk el al., 2014). In this
358 study, the Index of Lateritization (IOL) method was chosen following extensive work
359 characterizing degrees of alteration through BB and SQ profiles (Table 4, Widdowson et al.,
360 2007, 2009; Babechuk et al. 2014). These studies analysed samples from both sequences

using methods developed by Schellman (1986), based on SiO_2-Al_2O_3-Fe_2O_3 tri-plots. Regions on the ternary diagram are separated into degrees of alteration, ranging from unaltered protolith values, through the "limit of kaolinization" and then defining weak, moderate and strong lateritization (Widdowson, 2009). The limits of kaolinization occur at ~43 wt% SiO2 for BB and at ~57 wt% SiO_2 and a common lateritization process is proposed across western India (Widdowson, 2007, 2009; Wimpenny, 2007; Babechuk et al., 2014). For both profiles, the IOL is shown to be representative of general trends in degree of lateritization (when accounting for environmental conditions) and so the following equation is applied:

$$Index\ of\ Lateritisation\ (IOL) = 100 \times \frac{Al_2O_3 + Fe_2O_3}{SiO_2 + Al_2O_3 + Fe_2O_3}$$

Two general features are observed in the profiles of Tl and ε^{205}Tl variation with depth (Fig. 4b and Fig. 6). Firstly, there is a general upsection trend in each profile. In the case of the SQ profile, the upsection Tl concentrations become increasingly depleted with respect to the protolith when normalised to Zr and ε^{205}Tl become more positive. The BB profile displays different behaviour upsection, with generally increasing concentrations of Tl associated with a shift towards heavy ε^{205}Tl, however, this sample set is much more limited.

Secondly, the most distinctive feature of both profiles is the significant Tl enrichment at specific horizons, at 6 m in the BB profile (BB7) and 7.5 m in the SQ profile (SQ11) (Fig. 6). Due to the differences in magnitude and direction of the two features it is likely that two distinct processes are responsible, and they are thus discussed separately in the following sections (see Sections 4.1 and 4.2).

4.1. Behaviour of Tl and isotope fractionation of Tl during in-situ lateritic weathering

Firstly, the role of in-situ weathering on Tl and Tl stable isotopes can be examined through comparing the IOL with Tl concentration and ε^{205}Tl (Fig. 8 and Fig. 9), excluding the

386 heavy ε^{205}Tl samples (SQ11 and BB5) which will be discussed in section 4.2. For Tl
387 behaviour in the SQ profile, weak negative correlations are observed between Tl
388 concentration and ε^{205}Tl (R^2 = 36 %). This correlation is stronger between τ-$_{Tl/Zr}$ and ε^{205}Tl
389 (Fig. 10; R^2 = 57 %). This could imply that a vertical mixing mechanism could be partly
390 responsible for the range of ε^{205}Tl observed, between a higher concentration end-member
391 with ε^{205}Tl ~ < – 2.0 and a lower concentration, heavier reservoir with ε^{205}Tl ~ 0. This
392 vertical redistribution is possible within the SQ profile where most of the weathered samples
393 overlying the greywacke protolith (SQ2) show Tl depletions relative to the protolith (Fig. 4a)
394 and maybe be significant in Zone I (Fig. 10). To investigate whether the driver for this
395 redistribution is weathering intensity, the Tl profile is compared to IOL (Fig. 8). The limit of
396 kaolinization for the SQ profile occurs at ~ 57% SiO_2, below which desilicification starts and
397 the extent of lateritization can be classified by increasing intensity. Slight variance in the
398 metagreywacke protolith will also affect starting Fe- and Si- content, with protolith
399 compositions ranging between ~ 15 – 25% SiO_2. There is a strong positive correlation (R^2 =
400 98%) between an increase in IOL with Tl concentration for samples with IOL < ~25, before
401 substantial desilicification and Fe- enrichment occur. Above this limit, for kaolinized and
402 lateritized samples, any linear correlation ceases. This shift into kaolinization and
403 lateritization coincides with the breakdown of primary mineralogy (largely silicates) and the
404 formation of neo-clays and Fe- and Al-enrichment secondary phases (Widdowson, 2009). We
405 propose that the distinct shift in the Tl concentration-IOL relationship at this horizon reflects
406 mineralogical changes. Breakdown of primary mineralogy above ~20m likely allows for the
407 remobilization and transportation of Tl vertically, for example concentrating at 22.5m (SQ5,
408 652 ng/n Tl), or for removal of Tl laterally by groundwaters. Overall the τ-$_{Tl/Zr}$ values for the
409 SQ profile indicate an overall loss of Tl from the profile.

Within the BB profile the relationship between Tl mobility and degree of lateritization is much less distinct. The τ-$_{Tl/Zr}$ values from this profile show that there has been significant enrichment of Tl above protolith values and an overall addition of Tl. External inputs of Tl likely play a considerable role in the Tl concentration pattern for this profile and potential sources are discussed in Section 4.2.

In order to investigate Tl and Tl isotope behaviour during further lateritization and associated mineralogical changes, it is useful to compare its concentration profile and mobility with other major and trace elements.

Through the SQ profile, when water table sample SQ11 is not considered, very strong correlations (R^2 > 80 %) are observed for Zr-normalised concentrations of Rb (99 %), Li (97 %), Cs (96 %), Co (96 %) and Zn (95 %). This is matched by very strong major element correlations with MgO and K_2O. When sample SQ11 is included, Tl concentrations in the full SQ profile shows strong correlations (R^2 > 80 %) for Zn (96 %), Ba (87 %), Lu (85 %) and Co (83 %). Within the BB profile, when including supplementary trace element data, strong correlations are only observed for Ba (95 %) and Pb (85 %). These correlations in BB are maintained when palaeowater table horizons are removed from the analysis. When the mobility of elements (τ-$_{i/Zr}$) is considered rather than normalised concentration, $\tau_{Tl/Zr}$ shows positive correlation with $\tau_{Ba/Zr}$ (87 %) in SQ and $\tau_{Ba/Zr}$ (88 %) and $\tau_{Pb/Zr}$ (87 %) in BB. This suggests that when considering in-situ weathering processes alone, Tl behaviour is largely comparable to that of the alkali metals which share similarly large ionic radii (Shaw, 1952; Heinrichs et al., 1980; Babechuk et al., 2014; Nielsen et al., 2017a). The major host of these elements in primary minerals include a large suite of K-bearing minerals, particularly micas and feldspars (Prinz, 1967; Heinrichs et al., 1980). During weathering and lateritization the breakdown of these minerals commonly forms secondary clays, such as smectites. The alkali earths are commonly associated with these clays as they can adsorb onto the mineral surfaces

435 or substitute into interlayer sites. Studies of other laterite complexes have observed the
436 preferential retention of Ba on clay minerals when compared with the other alkaline earths
437 and alkali metals (e.g. Nesbitt et al., 1980; Das and Krishnaswami, 2007; Buggle et al.,
438 2011). Furthermore, Ba can also be retained by secondary Fe- and Mn-oxides (e.g. Das and
439 Krishnaswami, 2007; Bonnet et al., 2014). In both profiles the uppermost sections of the
440 laterite, the duricrust and indurated cap, represent the development of secondary Fe-minerals
441 dominated horizons, though the highest Fe-enrichments are observed near the inferred
442 palaeowater tables.

443 Thallium stable isotopes also show IOL-dependent behaviour (Fig. 9). Below 12 m
444 depth, where samples are unaltered to weakly lateritized, a weak positive correlation (R^2 =
445 56%) is observed between the degree of lateritization and ε^{205}Tl (Zones I and II: Fig. 9). This
446 general trend could be driven by the preferential removal of isotopically-light ^{203}Tl during the
447 early stages of kaolinization. Above this depth samples are strongly lateritized, with IOL
448 ranging from 80 – 86, and display relatively static ε^{205}Tl values of − 1.2 to − 1.0, with the
449 exception of palaeowater table samples discussed in Section 4.2. This could imply that a
450 threshold in the preferential mobilization of ^{203}Tl is reached during the stages of intense
451 lateritization. This threshold in preferential removal of ^{203}Tl is supported by comparable
452 trends in the relationship between ε^{205}Tl and τ-$_{Tl/Zr}$ (Fig. 10), which show a weak correlation
453 between loss of Tl and increasingly heavy Tl isotope composition. When ε^{205}Tl is compared
454 to Zr-normalised elemental concentrations, no strong correlations with any of the measured
455 elements are observed in SQ. Furthermore, while weathering can account for the isotopic
456 variations of ε^{205}Tl = − 2.2 to + 0.3 observed through the section, this process cannot
457 adequately explain the significant and common excursive nature of both the horizons
458 proximal to the water tables.
459

460 *4.2. Tl-enriched and heavy $\varepsilon^{205}Tl$ horizons*

461 Overall, variations in Tl concentrations interrogated using τ-values show a net enrichment
462 of Tl in the basaltic BB profile and a net loss from the greywacke-based SQ profile (Table 4).
463 All four measured horizons in the basaltic laterite show evidence for an external source of Tl,
464 with Tl concentrations exceeding protolith levels (Fig. 7b). For the greywacke-based SQ
465 profile all samples except SQ5 and SQ11 indicate a loss of Tl relative to the protolith
466 concentration of SQ2. The high Tl concentration of the unaltered SQ protolith means that
467 there would be sufficient Tl within the SQ profile that the concentration pattern observed
468 with depth could theoretically be explained using a simple model closed-system
469 redistribution of Tl. The relationship between degree of lateritization and Tl mobility in SQ
470 challenges this theory, however. A distinct shift in IOL in the SQ profile is observed between
471 12 m – 8.5 m depth (Table 4), which is recognized by Widdowson (2007) as the transition
472 between the kaolinized zone below and the strongly lateritized region above. If weathering
473 were the main process driving Tl concentration variations, we would expect to observe a
474 strong correlation between weathering intensity (IOL) and Tl mobility ($\tau_{Tl/Zr}$) (Fig. 11). The
475 absence of any systematic relationship between the two therefore supports the addition of
476 allochthonous Tl is also likely to the SQ profile too.
477
478 *4.2.1. Aeolian Tl fluxes to laterites*

479 Numerous studies investigating elemental mobility within the BB profile show
480 geochemical evidence for significant aeolian dust influxes, supported by $^{87}Sr/^{86}Sr$,
481 $^{143}Nd/^{144}Nd$, Li-isotopes, Re/Os ratios and high field strength element systematics
482 (Mason,1999; Kisakürek et al., 2004; Wimpenny et al., 2007; Babechuk, 2015). Wimpenny et
483 al. reported that Re/Os ratios of lateritized samples in SQ were sufficiently less radiogenic
484 than parent values, also suggesting that external inputs were likely significant. It was

485 postulated that the most likely dust source region for both sequences would be from the
486 surrounding Dharwar Craton, a complex of Archean to Proterozoic greywackes, mafic to
487 ultramafics and metabasic rocks (Klootwijk and Peirce, 1979; Devaraju et al., 2010). While
488 variations in Tl concentration are likely affected by external inputs to the profile, the
489 attribution of the heavy ε^{205}Tl excursions in both of the BB and SQ profiles to influxes of
490 allochthonous aeolian Tl requires a source reservoir of heavy ε^{205}Tl. However, the
491 geographical locations and differing ages of the laterite profiles does not support the input of
492 exotic materials with very different ε^{205}Tl values over a ~40 Myr time period. The basaltic
493 BB sequence lies within the laterally extensive and geochemically uniform Ambenali Fm
494 (Widdowson and Gunnell, 1999a, 1999b) and the SQ sequence lies within the Dharwar
495 Supergroup of metamorphosed greywackes. Aside from the distinct heavy horizons recorded
496 in this study, no other isotopically heavy terrestrial reservoirs of Tl have been reported.
497 Investigations into the Tl isotope characteristics of terrestrial reservoirs have shown relatively
498 uniform averages for loess and river particles, and hence continental crust, of $\varepsilon^{205}\text{Tl} = -2.0 \pm$
499 0.5 (Nielsen et al., 2005; Nielsen et al., 2006a; Nielsen et al., 2006b). Furthermore, Os
500 isotope studies indicate that aeolian fluxes alone cannot account for the total influx budget of
501 Os, so the potential role of cosmic dust was suggested (Wimpenny et al., 2007). Since the
502 formation of both the BB and SQ laterites it was estimated that cosmic dust could account for
503 <1 % of the total Os content observed in each profile. Given comparable concentrations of Tl
504 and Os in both cosmic dust (~50 ng/g) and the laterite profiles (Ander and Grevasse, 1989;
505 Wimpenny et al., 2007; Baker et al., 2010), it follows that the cosmic dust flux of Tl to
506 laterites is unlikely to explain the large Tl enrichments above unweathered substrate
507 concentrations observed in BB and SQ.

508 Overall these observations suggest that Tl concentrations within the profile have
509 likely been affected by the influx of aeolian material, particularly within the BB laterite. In

510 contrast, the large variations in the ε^{205}Tl profile are unlikely to be solely driven by aeolian
511 inputs. We suggest that the Tl isotope systematics within the laterites are likely further
512 influenced by groundwaters.
513
514 4.2.2. *The role of the palaeowater table*
515 Comparable Tl stable isotope fractionations are observed proximal to the inferred
516 palaeowater table in both laterite sequences of differing substrate age and lithology, age of
517 lateritization, and location (Fig. 4b). This striking similarity between two very different
518 laterite profiles implies a common process or environment as a driver of Tl stable isotope
519 fractionation. Both laterite profiles in this study contain a high abundance of Fe
520 oxides/oxyhydroxides (Table 1, and Fig. 3), particularly hematite and goethite, as well as
521 clays such as kaolinite in the upper sections (Wimpenny et al., 2007). This mineral
522 assemblage is common to many laterites of similar substrates (e.g. Ma et al., 2007;
523 Widdowson, 2007; Fernández-Caliani and Cantano, 2010). Whilst these minerals are
524 abundant across large sections of the profiles, over a thickness of approximately 10 m, the
525 heavy ε^{205}Tl excursions occur in discrete horizons, ≤5 m thick (Table 1 and Fig. 4b). Several
526 studies have highlighted elemental enrichment patterns and isotopic excursions that support
527 the existence of a palaeowater table (Mason, 1999; Kisakürek et al., 2004; Wimpenny et al.,
528 2006; Widdowson, 2007). This horizon and capillary zones coincide with samples SQ10 and
529 SQ11 and BB5 and BB6. Water tables within laterites form boundary horizons, below which
530 conditions are generally suboxic and above which conditions are oxic and susceptible to the
531 influx of oxic rainwater (e.g. Wimpenny et al., 2007). Open-system conditions allow for the
532 lateral movement and transport of ions in solution and play a key role in the alteration
533 minerals formed. For example, reduced conditions allow for the reduction of Fe(III) to
534 soluble Fe(II) species below the palaeowater table, whereas the transition to oxic conditions

535 above the water table can oxidise Fe(II) to Fe(III) and trigger Fe-oxide precipitation
536 (Kisakürek et al., 2004). These palaeowater tables can therefore superimpose further
537 mineralogical and elemental alteration on weathering profiles, in addition to providing an
538 allochthonous flux.

539 Within the SQ and BB profiles, correlations in elemental behaviour have highlighted
540 the likely importance of primary and secondary mineralogy during weathering on Tl
541 concentration. For both profiles, the strong correlation between Tl and Ba in particular
542 appears unaffected by changes in conditions at the palaeowater tables (Fig. 5). In surface
543 weathering environments two main phases are important in the cycling of Ba; Fe- and Mn-
544 oxides and phyllosilicates. Few detailed studies have been carried out on mineral-specific
545 fractionation for Tl stable isotopes. The largest isotopic fractionations for heavy element
546 systems like Tl have been predicted where nuclear field shift effects occur (Bigeleisen, 1996;
547 Schauble, 2007). Both the nuclear field shift effect and mass-dependent fractionation enrich
548 the more oxidized Tl(III) species in the heavier ^{205}Tl isotope, when Tl(III) is in equilibrium
549 with reduced Tl(I) (Schauble, 2007). Under the conditions of most surface environments
550 Tl(I) dominates as the more thermodynamically stable species (Law and Turner, 2011). One
551 environment where Tl(III) has been both predicted and observed is at the mineral surfaces of
552 specific Mn-oxides (Peacock and Moon, 2012; Nielsen et al., 2013). There is widespread
553 evidence of the preferential association of Tl with Mn-oxides in both terrestrial and marine
554 reservoirs, through Tl substitution with K and adsorption-oxidation reactions (e.g.
555 Rehkämper and Nielsen, 2004; Vaněk et al., 2011; Kersten et al., 2014). Hydrogenetic FeMn
556 crusts display large positive ε^{205}Tl values of up to ~+ 14 epsilon units (Rehkämper et al.,
557 2002; Nielsen et al. 2017a), similar to those observed in this study within the terrestrial
558 realm. Peacock and Moon (2012) attribute the FeMn crust Tl isotope signature to the
559 adsorption and oxidation of Tl(I) to Tl(III) during inner-sphere complexation onto hexagonal

560 birnessite (Hx-birnessite). Thallium isotope fractionation is not observed within the limited
561 other Mn-oxides which have been measured, including todorokite and vernadite (e.g.
562 Peacock and Moon, 2012). Other mineral species are known to be important host phases
563 within soil complexes. For example, Tl(I) uptake by illite-type clays has been observed, with
564 Tl substituting for K in illite (e.g. Voegelin et al., 2015). Further focused studies on potential
565 mineral-specific fractionation effects are required to investigate whether interaction with
566 illite-type clays can cause significant fractionation of Tl stable isotopes.

567 The strikingly heavy ε^{205}Tl signals at the paleo water table horizons are of the same
568 magnitude and direction as the Tl isotope fractionations observed in the FeMn crusts,
569 attributed to Hx-birnessite (Peacock and Moon, 2012). In particular, within the SQ profile
570 this heavy ε^{205}Tl excursion coincides with peaks in Tl, Mn and Fe_2O_3 content. Furthermore,
571 the shift to higher Fe_2O_3 begins just below the Tl peak, within sample SQ10, whereas the
572 peak in Tl and Mn concentration coincide distinctly within SQ11. Therefore, we suggest that
573 the ε^{205}Tl variation within the SQ laterite may reflect changing Mn-mineralogy. Through the
574 majority of the profile the presence of todorokite or similar Mn-oxides, which are not
575 associated with a Tl isotope fractionation, could occur via the transformation of birnessite. At
576 the palaeowater tables, oxidative conditions could thus inhibit the transformation of birnessite
577 to todorokite. Higher oxidation states have been proposed to alter the structure of birnessite,
578 impeding the initiation of the first step in the four-stage birnessite to todorokite
579 transformation (Cui et al., 2008; Cui et al., 2009).

580 Within the BB profile the heaviest ε^{205}Tl horizon coincides with the highest Fe_2O_3
581 content but peaks in Tl and Mn concentration occur 2m higher in the profile. This may
582 suggest that Mn-oxide mineralogy may not be the dominant control on Tl behaviour in this
583 profile. Thus, whilst we speculate that the positive Tl isotope excursions at the palaeowater
584 tables are due to the presence of birnessite instead of todorokite, the Tl concentrations within

585 the laterite sequences are insufficient to quantitatively determine the diagnostic 7 and 10 Å
586 spacings using X-ray absorption spectroscopy (Peacock and Moon, 2012). Thallium
587 fractionation at comparable concentrations has been investigated using sequential extraction
588 methods (e.g. Vaněk et al., 2009; Vaněk et al., 2011). Given the magnitude of natural
589 variations observed in the laterite profiles, exploration of the specific mineral phase(s)
590 associated with Tl isotope fractionation is a fruitful avenue for future research.
591

592 **5. CONCLUSIONS**

593 This study provides the first characterization of Tl concentrations and stable isotope
594 compositions within lateritic weathering profiles. Thallium concentrations range between 7 –
595 244 ng/g for the Bidar basaltic-based profile and 37 – 652 ng/g for the Goan greywacke-
596 based profile. Considerable variation in Tl stable isotope ratios were observed, from – 2.4 to
597 + 6.2. In particular, distinct heavy ε^{205}Tl excursions at or near palaeowater table horizons
598 highlight the need to characterize the Tl isotope systematics of surface reservoirs to improve
599 our understanding of Tl cycling in surface environments. In addition, there is a small (~1 – 2
600 epsilon units) but discernible effect of continental weathering on Tl isotopes. Thus, both
601 weathering and horizons of enhanced fluid circulation such as paleo-water tables are likely to
602 impact primary ε^{205}Tl values, for example from industrial pollution processes (Kersten et al.,
603 2014). Further characterization of natural surface processes and other potential
604 mineralogically driven mechanisms of Tl stable isotope fractionation is required before the
605 effects of anthropogenically driven-Tl isotope variations can be fully assessed.
606 The processes that occur at the palaeowater table of weathering profiles are complex,
607 with numerous documented excursions in elemental concentrations and isotopic values. This
608 regime has a significant effect upon the availability and flux of the elements to the wider
609 groundwater and associated fluvial systems. The BB profile highlights the importance of

610 external fluxes of Tl to weathering profiles developed on low-Tl substrates. There is also
611 strong evidence for the role of groundwater in the redistribution of redox sensitive elements
612 and the formation of alteration minerals. These processes have resulted in fractionations of ~
613 + 6 ε^{205}Tl from the profile averages proximal to the palaeowater table, regardless of location,
614 lithology, age and timing of lateritization. A mechanism of mineralogically driven Tl isotope
615 fractionation, similar to that of Mn-oxides in marine FeMn crusts (Peacock and Moon, 2012)
616 could result in heavy ε^{205}Tl signatures at redox boundaries, such as the palaeowater table
617 horizon in the SQ profile. To improve the understanding of Tl and Tl stable isotope
618 behaviour in surface environments, further work is required to characterize the mineral-
619 specific behaviour of Tl.
620
621 Acknowledgements
622 We thank three anonymous reviewers and editorial handling by Jan Wiederhold for helpful
623 comments that significantly improved prior versions of this manuscript. This work formed
624 the basis of SH's final year undergraduate thesis at Imperial College London. Barry Coles
625 and Katharina Kressig are gratefully acknowledged for their efforts in keeping the mass
626 spectrometers and clean labs functioning, respectively. Sophie Munson is thanked for her
627 help with trace element digestions. SHL acknowledges support from the Leverhulme Trust
628 and a NERC independent research fellowship.
629

630 # 6. REFERENCES

631 Anders E. and Grevesse N., (1989) Abundances of the elements: meteoritic and solar.
632 *Geochimica et Cosmochimica Acta,* **53**, 197–214.
633 Babechuk M. G., Widdowson M. and Kamber B. S. (2014) Quantifying chemical weathering
634 intensity and trace element release from two contrasting basalt profiles, Deccan Traps,
635 India. *Chemical Geology*, **363**, 56–75.

636 Babechuk M. G., Widdowson M., Murphy M. and Kamber B. S. (2015) A combined Y/Ho,
637 high field strength element (HFSE) and Nd isotope perspective on basalt weathering,
638 Deccan Traps, India. *Chemical Geology*, **396**, 25–41.
639 Baker R. G. A., Rehkämper M., Ihlenfeld C., Oates C. J., Coggon R. M. (2010) Thallium
640 isotope variations in an ore-bearing continental igneous setting: Collahuasi formation,
641 Northern Chile. *Geochimica et Cosmochimica Acta*, **74**, 4405-4416.
642 Berger A. and Frei R. (2014) The fate of chromium during tropical weathering: A laterite
643 profile from Central Madagascar. *Geoderma*, **213**, 521–532.
644 Bigeleisen J. (1996) Temperature dependence of the isotope chemistry of the heavy elements.
645 *Proceedings of the National Academy of Sciences*, **93**, 9393–9396.
646 Bonnet N. J., Beauvais A., Arnaud N., Chardon D., and Jayananda M. (2014) First
647 40Ar/39Ar dating of intense Late Palaeogene lateritic weathering in Peninsular India.
648 *Earth and Planetary Science Letters*, **386**, 126–137.
649 Borger H. and Widdowson M. (2001) Indian laterites, and lateritious residues of southern
650 Germany: a petrographic, mineralogical, and geochemical comparison. *Zeitschrift fur*
651 *Geomorphologie*, **45**, 177–200.
652 Buggle B., Glaser B., Hambach U., Gerasimenko N., and Marković S. (2011) An evaluation
653 of geochemical weathering indices in loess-paleosol studies. *Quaternary International*,
654 **240**, 12–21.
655 Bullen T.D. (2012) Stable Isotopes of Transition and Post-Transition Metals as Tracers in
656 Environmental Studies. In *Handbook of Environmental Isotope Geochemistry.*
657 *Advances in Isotope Geochemistry* (ed. Baskaran M.). Springer, Berlin, Heidelberg
658 Chadwick O. A., Brimhall G. H., and Hendricks D. M., (1990) From a black to a gray box -
659 mass balance interpretation during pedogenesis. *Geomolphology*, **3**, 369 – 390.
660 Cui H., Liu X., Tan W., Feng X., Liu F., and Ruan H. D. (2008) Influence of Mn (III)
661 availability on the phase transformation from layered buserite to tunnel-structured
662 todorokite. *Clays and Clay Minerals*, **56**, 397–403.
663 Cui H., Qiu G., Feng X., Tan W., and Liu F. (2009) Birnessites with different average
664 manganese oxidation states synthesized, characterized, and transformed to todorokite at
665 atmospheric pressure. *Clays and Clay Minerals*, **57**, 715–724.
666 Dequincey O., Chabaux F., Clauer N., Sigmarsson O., Liewig N., and Leprun J. C. (2002)
667 Chemical mobilizations in laterites: Evidence from trace elements and ^{238}U-^{234}U-^{230}Th
668 disequilibria. *Geochimica et Cosmochimica Acta*, **66**, 1197–1210.
669 Das, A. and Krishnaswami, S. (2007). Elemental geochemistry of river sediments from the
670 Deccan Traps, India: Implications to sources of elements and their mobility during
671 basalt-water interaction. *Chemical Geology*, **242**, 232–254.
672 Devaraju T. C., Sudhakara T. L., Kaukonen R. J., Viljoen R. P., Alapieti T. T., Ahmed S. A.,
673 and Sivakumar S. (2010). Petrology and geochemistry of greywackes from Goa-
674 Dharwar sector, western Dharwar craton: Implications for volcanoclastic origin.
675 *Journal of the Geological Society of India*, **75**, 465–487.
676 Fedo C. M., Nesbitt H. W. and Young G. M. (1995) Unravelling the effects of potassium-
677 metasomatism in sedimentary rocks and paleosols, with implications for weathering
678 conditions and provenance. *Geology,* **23**, 921–924.
679 Fernández-Caliani J. C. and Cantano M. (2010) Intensive kaolinization during a lateritic
680 weathering event in South-West Spain; Mineralogical and geochemical inferences from
681 a relict paleosol. *Catena*, **80**, 23–33.
682 Gall L., Williams H. M., Siebert C., Halliday A.N., Herrington R.J. and Hein J.R. (2013)
683 Nickel isotopic compositions of ferromanganese crusts and the constancy of deep ocean
684 inputs and continental weathering effects over the Cenozoic. *Earth and Planetary*
685 *Science Letters*, **375**, 148–155.

686 Hein J. R., Koschinsky A., Bau M., Manheim F. T., Kand J. K. and Roberts L. (2000) Cobalt-
687 rich ferromanganese crusts in the Pacific. In *Handbook of Marine Mineral Deposits*
688 (ed. D. S. Cronan). CRC Press, London. pp. 239–278.
689 Heinrichs H., Schulz-Dobrick B., and Wedepohl K. H. (1980) Terrestrial geochemistry of Cd,
690 Bi, Tl, Pb, Zn and Rb. *Geochimica et Cosmochimica Acta*, **44**,1519–1533.
691 Huh Y., Chan L. H., Zhang L., and Edmond J. M. (1998) Lithium and its isotopes in major
692 world rivers: implications for weathering and the oceanic budget. *Geochimica et*
693 *Cosmochimica Acta*, **62**, 2039–2051.
694 Jacobson A. R., McBride M. B., Baveye P., and Steenhuis T. S. (2005) Environmental factors
695 determining the trace-level sorption of silver and thallium to soils. *Science of the Total*
696 *Environment*, **345**,191–205.
697 Jay A. E. and Widdowson M. (2008) Stratigraphy, structure and volcanology of the SE
698 Deccan continental flood basalt province: implications for eruptive extent and volumes.
699 *Journal of the Geological Society of London,* **165**, 177-188.
700 Jones L. H. P. and Milne A. A. (1956) Birnessite, a New Manganese Oxide Mineral from
701 Aberdeenshire, Scotland. *Mineralogical Magazine*, **31**, 283–288.
702 Kazantzis, G. (2000). Thallium in the environment and health effects. *Environmental*
703 *Geochemistry and Health,* **22**, 275–280.
704 Kersten M., Xiao T., Kreissig K., Brett A., Coles B. J. and Rehkämper M. (2014) Tracing
705 anthropogenic thallium in soil using stable isotope compositions. *Environmental*
706 *Science & Technology*, **48**, 9030–9036.
707 Kisakürek B., Widdowson M. and James R. H. (2004) Behaviour of Li isotopes during
708 continental weathering: The Bidar laterite profile, India. *Chemical Geology*, **212**, 27–
709 44.
710 Klootwijk C.T. and Peirce J.W., 1979. India's and Australia's pole path since the late
711 Mesozoic and the India–Asia collision. *Nature*, **282**, 605–607.
712 LaBrecque J. J. and Schorin H. (1987) Some statistical parameters for selected trace elements
713 in VL-1. *Zeitschrift für Geomorphologie*, **64**, 33–38.
714 Law S., and Turner A. (2011) Thallium in the hydrosphere of south west England.
715 *Environmental Pollution*, **159**, 3484 – 3489.
716 Liu S. A., Teng F. Z., Li S., Wei G. J., Ma J. L. and Li D. (2014) Copper and iron isotope
717 fractionation during weathering and pedogenesis: Insights from saprolite profiles.
718 *Geochimica et Cosmochimica Acta*, **146**, 59–75.
719 Ma J. L., Wei G. J., Xu Y. G., Long W. G. and Sun W. D. (2007) Mobilization and re-
720 distribution of major and trace elements during extreme weathering of basalt in Hainan
721 Island, South China. *Geochimica et Cosmochimica Acta*, **71**, 3223–3237.
722 Martini I. P. and Chesworth W. (1992) *Weathering, Soils and Paleosols*. Elsevier,
723 Amsterdam, pp. 407–443.
724 Mason T. F. D. (1999) A combined chemical, mineralogical and isotopic study of lateritic
725 soils from the Deccan Traps, S.W. India: implications for the processes which control
726 laterite development. Master of Research Thesis, University of Edinburgh, U.K.
727 Nesbitt H. W. and Young G. M. (1989) Formation and diagenesis of weathering profiles.
728 *Journal of Geology*, **97**, 129–147.
729 Nesbitt H. W., Markovics G., and Price R. G. (1980). Chemical processes affecting alkalis
730 and alkaline earths during continental weathering. *Geochimica et Cosmochimica Acta*,
731 **44**, 1659–1666.
732 Nielsen S. G., Rehkämper M., Baker J. and Halliday A. N. (2004) The precise and accurate
733 determination of thallium isotope compositions and concentrations for water samples
734 by MC-ICPMS. *Chemical Geology*, **204**, 109–124.

735 Nielsen S. G., Rehkämper M., Porcelli D., Andersson P., Halliday A. N., Swarzenski P. W.
736 and Günther D. (2005) Thallium isotope composition of the upper continental crust and
737 rivers - An investigation of the continental sources of dissolved marine thallium.
738 *Geochimica et Cosmochimica Acta*, **69**, 2007–2019.
739 Nielsen S. G., Rehkämper M., Norman M. D., Halliday A. N. and Harrison D. (2006a)
740 Thallium isotopic evidence for ferromanganese sediments in the mantle source of
741 Hawaiian basalts. *Nature*, **439**, 314–317.
742 Nielsen S. G., Rehkämper M., Teagle D. A. H., Butterfield D. A., Alt J. C. and Halliday A.
743 N. (2006b) Hydrothermal fluid fluxes calculated from the isotopic mass balance of
744 thallium in the ocean crust. *Earth and Planetary Science Letters*, **251**, 120–133.
745 Nielsen S. G., Mar-Gerrison S., Gannoun A., LaRowe D., Klemm V., Halliday A. N. and
746 Hein J. R. (2009) Thallium isotope evidence for a permanent increase in marine organic
747 carbon export in the early Eocene. *Earth and Planetary Science Letters*, **278**, 297–307.
748 Nielsen S. G., Goff M., Hesselbo S. P., Jenkyns H. C., LaRowe D. E. and Lee C. T. A. (2011)
749 Thallium isotopes in early diagenetic pyrite – A paleoredox proxy? *Geochimica et*
750 *Cosmochimica Acta*, **75**, 6690–6704.
751 Nielsen S. G., Wasylenki L. E., Rehkämper M., Peacock C. L., Xue Z. and Moon E. M.
752 (2013) Towards an understanding of thallium isotope fractionation during adsorption to
753 manganese oxides. *Geochimica et Cosmochimica Acta*, **117**, 252–265.
754 Nielsen S. G., Yogodzinski G., Prytulak J., Plank T., Kay S. M., Kay R. W., Blusztajn J.,
755 Owens, J. D., Auro M. and Kading T. (2016). Tracking along-arc sediment inputs to the
756 Aleutian arc using thallium isotopes. *Geochimica et Cosmochimica Acta*, **181**, 217–
757 237.
758 Nielsen S. G., Rehkämper M. and Prytulak J. (2017a) Investigation and application of
759 thallium isotope fractionation. *Reviews in Mineralogy and Geochemistry,* **82**, 759–798.
760 Nielsen S. G., Prytulak J., Blusztajn J., Shu Y., Auro M., Regelous M. and Walker J. (2017b)
761 Thallium isotopes as tracers of recycled materials in subduction zones: review and new
762 data from Tonga-Kermadec and Central America. *Journal of Volcanology and*
763 *Geothermal Research,* **339**, 23–40.
764 Pavlícková J., Zbíral J., Smatanová M., Habarta P., Houserová P. and Kubán V. (2006)
765 Uptake of thallium from naturally-contaminated soils into vegetables. *Food Additives*
766 *and Contaminants*, **23**, 484–91.
767 Peacock C. L., Moon E. M., Nielsen S. G. and Halliday A. N. (2009) Oxidative scavenging
768 of Tl by Mn oxide birnessite: Sorption and stable isotope fractionation. *Goldschmidt*
769 *Conference Proceedings Supplement 1*, A1003.
770 Peacock C. L. and Moon E. M. (2012) Oxidative scavenging of thallium by birnessite:
771 Explanation for thallium enrichment and stable isotope fractionation in marine
772 ferromanganese precipitates. *Geochimica et Cosmochimica Acta*, **84**, 297–313.
773 Poitrasson F., Viers J., Martin F. and Braun J.-J. (2008) Limited iron isotope variations in
774 recent lateritic soils from Nsimi, Cameroon: implications for the global Fe geochemical
775 cycle. *Chemical Geology*, **253**, 54–63.
776 Prinz, M. (1967). Geochemistry of basaltic rocks: trace elements. In: *Basalts* (Ed. Hess H. H.
777 and Poldervaart A.). Interscience Publishers, p. 482
778 Prytulak J., Nielsen S. G., Plank T., Barker M. and Elliott T. (2013) Assessing the utility of
779 thallium and thallium isotopes for tracing subduction zone inputs to the Mariana arc.
780 *Chemical Geology*, **345**, 139–149.
781 Rehkämper M. and Halliday A. N. (1999) The precise measurement of Tl isotopic
782 compositions by MC-ICPMS: Application to the analysis of geological materials and
783 meteorites. *Geochimica et Cosmochimica Acta*, **63**, 935–944.

784 Rehkämper M., Frank M., Hein J. R., Porcelli D., Halliday A., Ingri J. and Liebetrau V.
785 (2002) Thallium isotope variations in seawater and hydrogenetic, diagenetic, and
786 hydrothermal ferromanganese deposits. *Earth and Planetary Science Letters*, **197**, 65–
787 81.
788 Rehkämper M. and Nielsen S. G. (2004) The mass balance of dissolved thallium in the
789 oceans. *Marine Chemistry*, **85**, 125–139.
790 Schauble E. A. (2007) Role of nuclear volume in driving equilibrium stable isotope
791 fractionation of mercury, thallium, and other very heavy elements. *Geochimica et*
792 *Cosmochimica Acta*, **71**, 2170–2189.
793 Schellmann W., (1986) A new definition of laterite. In *Lateritisation Processes. Memoirs of*
794 *the Geological Survey of India 120* (ed. P. K. Banerji). Order of the Governor-General
795 of India, India, pp. 1–7.
796 Schmidt P. W., Prasad V. and Ramam P. K. (1983) Magnetic ages of some Indian laterites.
797 *Palaeogeography, Palaeoclimatology, Palaeoecology*, **44**, 185-202.
798 Schorin H. and LaBrecque J. J. (1983) A laterite standard reference material: Venezuelan
799 Laterite VL-1. *Geostandards Newsletter*, **7**, 233–242.
800 Shaw D. M. (1952) The geochemistry of thallium. *Geochimica et Cosmochimica Acta*, **2**,
801 118–154.
802 Tardy Y. (1997) Petrology of Laterites and Tropical Soils. A.A. Balkema, Rotterdam.
803 Taylor S. R., McLennan S. M. (1985) The continental crust: its composition and evolution.
804 Blackwell Scientific Publication, Carlton.
805 Teng F.-Z, Watkins J. M., and Dauphas, N. (2017) Non-Traditional Stable Isotopes. *Reviews*
806 *in Mineralogy & Geochemistry*, **82**.
807 Vaněk A., Chrastný V., Mihaljevič M., Drahota P., Grygar T. and Komárek M. (2009)
808 Lithogenic thallium behavior in soils with different land use. *Journal of Geochemical*
809 *Exploration*, **102**, 7–12.
810 Vaněk A., Komárek M., Vokurková P., Mihaljevič M., Šebek O., Panušková G. and Drábek
811 O. (2011) Effect of illite and birnessite on thallium retention and bioavailability in
812 contaminated soils. *Journal of Hazardous Materials*, **191**, 170–176.
813 Vaněk A., Grösslová Z., Mihaljevič M., Trubač J., Ettler V., Teper L., Cabala J., Rohovec J.,
814 Zádorová T., Penížek V., Pavlů L., Holubík O., Němeček K., Houška J., Drábek O. and
815 Ash C. (2016) Isotopic Tracing of Thallium Contamination in Soils Affected by
816 Emissions from Coal-Fired Power Plants. *Environmental Science & Technology*, **50**,
817 9864–9871.
818 Vaněk, A., Grösslová, Z., Mihaljevič, M., Ettler, V., Trubač, J., Chrastný, V., Penížek, V.,
819 Teper, L., Cabala, J., Voegelin, A., Zádorová, T., Oborná, V., Drábek, O., Holubík, O.,
820 Houška, J., Pavlů, L., and Ash, C. (2018). Thallium isotopes in metallurgical
821 wastes/contaminated soils: A novel tool to trace metal source and behavior. *Journal of*
822 *Hazardous Materials*, **343**, 78–85.
823 Voegelin A., Pfenninger N., Petrikis J., Majzlan J., Plötze M., Senn A. C., Mangold S.,
824 Steininger R. and Göttlicher J. (2015) Thallium speciation and extractability in a
825 thallium- and arsenic-rich soil developed from mineralized carbonate rock.
826 *Environmental Science and Technology*, **49**, 5390–5398.
827 Wiederhold J. G. (2015) Metal stable isotope signatures as tracers in environmental
828 geochemistry. Environmental Science and Technology, 49, 2606–2624.
829 Widdowson M. (2007) Laterite and Ferricrete. In: *Geochemical Sediments and Landscapes*
830 (eds. D. J Nash and S. J. McLaren). Wiley-Blackwell, Oxford, pp. 46–94.
831 Widdowson M. (2009) Evolution of Laterite in Goa. In: *Natural Resources of Goa: A*
832 *Geological Perspective (*eds. A. Mascarenhas G. Kalavampara). Geological Survey of
833 India, India, pp. 35-68.

834 Widdowson M. and Cox K. G. (1996) Uplift and erosional history of the Deccan traps, India:
835 Evidence from laterites and drainage patterns of the Western Ghats and Konkan Coast.
836 *Earth and Planetary Science Letters*, **137**, 57-69.
837 Widdowson M., and Gunnell Y. (1999a) Tertiary palaeosurfaces and lateritization of the
838 coastal lowlands of Western Peninsula India. In *Palaeoweathering, Palaeosurfaces and*
839 *Related Continental Deposits, Special Publication*. International Association of
840 Sedimentologists, Gent. pp. 245-274.
841 Widdowson M. and Gunnell Y. (1999b) Lateritization, geomorphology and geodynamics of a
842 passive continental margin: The Konkan and Kanara coastal lowlands of western
843 Peninsular India. In: *Palaeoweathering, Palaeosurfaces and Related Continental*
844 *Deposits. Special Publication 27, International Association of Sedimentologists* (eds.
845 M. Thiry, R. Simon-Coinçon). Blackwell, Oxford, pp. 245–274.
846 Widdowson M. (1997). The geomorphological and geological importance of palaeosurfaces.
847 *Geological Society, London, Special Publications,* **120**, 1–12.
848 Wimpenny J., Gannoun A., Burton K. W., Widdowson M., James R. H. and Gíslason S. R.
849 (2007) Rhenium and osmium isotope and elemental behaviour accompanying laterite
850 formation in the Deccan region of India. *Earth and Planetary Science Letters*, **261**,
851 239–258.
852 Xiao T., Guha J., Boyle D., Liu C. Q., Zheng B., Wilson G. C. and Chen J. (2004) Naturally
853 occurring thallium: A hidden geoenvironmental health hazard? *Environment*
854 *International*, **30**, 501–507.

855 **TABLES**

856 *Table 1 Thallium concentrations and $\varepsilon^{205}Tl$ from MC-ICPMS (Imperial College London) and ICP-MS (Open University) analyses of the basaltic BB and*
857 *greywacke SQ laterite sequences. A standard error of ±0.4 $\varepsilon^{205}Tl$ from long-term reproducibility is applied except in cases where this value is exceeded.*

Sample	Depth (m)	Lithology	[Tl] ng/g MC-ICPMS	[Tl] ng/g ICP-MS	$\varepsilon^{205}Tl$	2sd	# runs	# dissolutions
SQ2	34.0	Unweathered greywacke	559	540	-2.3	0.4	5	1
SQ3	30.0	Lighter greywacke	459	444	-1.3	0.5	1	1
SQ4	25.5	Soft weathered greywacke	231	218	-2.4	0.6	2	1
SQ5	22.5	Weathered greywacke	700	652	-2.1	0.6	4	2
SQ6	15.0	Red weathered greywacke	340	324	-1.9	0.5	1	1
SQ7	14.0	Base of laterite	148	126	-1.1	0.5	7	4
SQ8	13.5	Nodular laterite base	76	105	-0.5	0.4	2	1
SQ9	12.0	Nodular laterite	95	81	+0.3	0.4	2	1
SQ10	8.5	Semi-indurated laterite	40	37	-1.2	0.4	2	1
SQ11	7.5	Massive laterite	456	544	+3.5	0.6	2	1
SQ12	3.5	Indurated laterite cap	103	105	-1.0	0.4	2	1
SQ13	2.5	Indurated laterite cap	127	135	-1.0	0.4	4	1
BB5: Average	13.0	Basaltic saprolite	24	26	+6.2	1.5	4	3
BB5: Separate Runs								
BB5-1			27		+5.3			
BB5-2			25		+5.9			
BB5-2			25		+6.4			
BB5-3			28		+7.1			
BB7	6.0	Base of laterite	252	244	+0.3	0.5	1	1
BB8	5.0	Nodular laterite	38	39	-0.5	0.4	3	2

858

Table 2 Thallium concentrations and $\varepsilon^{205}Tl$ of reference materials measured in this study from MC-ICPMS (Imperial College London) and ICP-MS (Open University) analyses and from literature.

Reference Materials		[Tl] ng/g MC-ICPMS	[Tl] ng/g ICP-MS	$\varepsilon^{205}Tl$	2sd	# runs	# dissolutions
AGV-2, This study	Andesitic USGS standard	222		-2.6	0.6	10	4
AGV-2, Nielsen et al., 2017a	Andesitic USGS standard	269		-3.0	0.6	8	8
BCR-2, This study	Basaltic USGS standard	255		-2.5	0.4	4	2
BCR-2, Nielsen et al., 2017a	Basaltic USGS standard	257		-2.5	0.4	4	4
VL2	Venezuelan laterite standard	29	30	+2.1	0.5	2	2

Table 3 Trace element concentrations determined by ICP-MS at the Open University (μg/g).

	BB3	BB5	BB7	BB8	SQ1	SQ2	SQ3	SQ4	SQ5	SQ6	SQ7	SQ8	SQ9	SQ10	SQ11	SQ12	SQ13	SQ14	VL1	VL2
Li	6.8	3.7	11.2	17.4	7.4	31.6	32.4	12.5	45.0	20.2	13.8	9.7	8.7	4.5	4.2	7.1	9.5	8.8	0.1	2.8
Sc	68	77	34	47	43	12	13	7	11	10	15	16	17	24	27	28	38	66	64	82
Ti	26903	29298	16215	11650	8522	3243	3391	1809	2922	2563	4129	4558	3836	8646	2857	10307	8624	9471	16771	15681
V	730	1997	704	992	366	99	102	56	94	84	121	143	138	852	112	578	822	788	775	587
Cr	206	261	228	744	115	109	118	63	79	83	87	112	125	720	166	720	946	749	98	25
Mn	775	395	2401	464	1941	1031	831	508	1404	413	429	162	99	130	3720	344	256	245	494	730
Co	67	14	40	18	63	19	19	6	20	10	11	3	3	3	38	8	5	6	7	38
Ni	305	73	63	102	90	42	47	15	41	23	69	42	38	69	147	58	59	58	6	37
Cu	446	519	228	196	122	50	40	66	37	53	42	38	34	31	52	39	50	61	105	255
Zn	126	72	62	74	127	112	115	33	146	66	38	38	23	21	97	25	25	31	60	99
Rb	1.24	0.83	1.57	4.12	18.32	126.77	108.53	46.57	147.69	79.03	40.83	31.17	26.86	9.02	16.31	22.07	28.07	27.59	0.37	1.37
Sr	14	6	16	10	243	117	113	104	86	113	7	9	7	21	40	40	35	41	1	1
Y	796	14	6	8	31	17	27	13	17	40	12	9	8	10	27	17	14	19	3	7
Zr	253	315	193	224	66	172	192	83	137	123	213	196	191	203	76	261	217	236	421	419
Nb	19.6	25.5	15.2	17.0	3.3	13.8	15.0	7.1	12.5	10.8	16.8	17.6	16.0	20.8	8.1	32.9	27.3	30.7	17.2	18.2
Sb	0.09	0.31	0.81	1.41	0.02	0.24	0.34	0.24	0.30	0.26	0.41	0.62	0.60	11.53	1.12	8.40	14.46	8.30	0.74	0.31
Cs	0.112	0.101	0.140	0.403	0.556	4.314	3.538	1.284	4.506	2.104	1.107	1.502	0.896	0.441	1.704	1.323	1.920	1.595	0.011	0.092
Ba	57	16	445	18	144	702	609	404	665	549	571	473	454	46	730	136	136	125	6	32
La	33.3	9.6	28.7	13.3	8.2	25.7	41.9	15.1	13.4	72.1	7.3	6.9	3.4	19.6	54.0	40.6	29.4	32.1	2.1	4.4
Ce	25.9	22.5	270.1	27.6	20.4	52.8	75.5	32.7	27.8	98.9	63.4	21.2	9.1	33.5	87.9	87.3	63.1	60.1	14.7	164.4
Pr	16.78	4.07	3.97	2.61	2.85	5.62	7.88	3.50	2.96	12.38	1.99	1.64	0.81	2.97	8.49	6.33	4.90	5.66	0.47	1.29
Nd	77.3	18.2	11.9	9.5	13.7	20.1	28.1	12.7	10.7	43.4	7.6	6.0	3.1	9.4	26.5	20.1	16.0	19.4	1.8	5.4
Sm	29.70	4.49	2.01	1.98	3.85	3.72	5.06	2.51	2.14	7.91	1.58	1.18	0.68	1.55	4.93	3.23	2.78	3.51	0.53	1.59
Eu	12.27	1.11	0.51	0.48	1.41	0.82	0.96	0.57	0.54	1.62	0.40	0.31	0.22	0.31	1.14	0.58	0.53	0.67	0.15	0.42
Gd	56.98	3.62	2.64	1.72	4.28	3.02	4.41	2.27	1.98	7.45	1.53	1.02	0.64	1.33	5.11	2.64	2.29	2.87	0.51	1.91
Tb	12.85	0.63	0.28	0.30	0.77	0.46	0.67	0.36	0.33	1.14	0.25	0.18	0.13	0.22	0.82	0.40	0.37	0.46	0.11	0.27
Dy	93.32	3.65	1.50	1.85	4.93	2.67	3.95	2.18	2.13	6.36	1.74	1.29	1.00	1.47	4.94	2.53	2.31	3.06	0.73	1.69
Ho	24.79	0.76	0.32	0.42	1.11	0.59	0.87	0.46	0.53	1.28	0.42	0.33	0.27	0.35	1.07	0.61	0.53	0.67	0.18	0.38
Er	64.05	1.97	0.84	1.14	3.07	1.84	2.59	1.32	1.77	3.40	1.42	1.11	0.94	1.13	2.96	1.87	1.68	2.04	0.55	1.13
Yb	53.87	1.99	0.90	1.27	2.89	2.23	2.75	1.32	2.24	2.97	1.95	1.59	1.44	1.47	2.98	2.26	1.95	2.37	0.77	1.54
Hf	7.03	8.47	5.20	5.73	1.82	4.63	5.09	2.29	3.65	3.22	5.67	5.22	5.21	5.48	2.10	7.05	5.82	6.16	11.73	11.32
Lu	8.29	0.30	0.14	0.20	0.45	0.35	0.42	0.20	0.40	0.42	0.32	0.28	0.25	0.22	0.46	0.37	0.31	0.38	0.13	0.25
Ta	1.44	1.72	1.53	1.16	0.19	1.36	1.45	0.61	1.03	1.06	1.73	1.64	1.53	1.48	0.62	3.08	1.78	2.30	1.14	1.18
Tl	0.007	0.026	0.244	0.039	0.075	0.540	0.444	0.218	0.652	0.324	0.126	0.105	0.081	0.037	0.544	0.105	0.135	0.129	0.006	0.030
Pb	2.30	10.43	46.46	19.19	2.77	12.85	12.75	11.62	13.97	10.78	28.09	17.68	15.26	31.24	29.10	54.60	42.17	35.84	7.99	39.02
Th	1.92	3.60	3.82	10.06	0.47	21.06	21.51	7.61	15.51	13.63	26.82	21.94	23.64	20.80	6.06	24.91	22.02	22.61	14.00	11.02
U	1.01	2.19	1.24	2.00	0.09	5.90	6.32	2.19	4.81	4.07	6.29	5.81	6.21	4.52	6.79	6.65	7.39	10.37	1.69	3.14
Sn	1.85	0.53	0.79	1.09	0.75	3.11	2.34	1.71	3.84	1.98	3.25	3.20	3.09	2.61	1.45	5.46	2.69	3.01	2.47	0.46

866 *Table 4 τ-values and Index of lateritization (IOL) values for BB and SQ profiles.*

Sample	Depth (m)	τ-value	IOL	Degree of lateritization (Widdowson 2007)
BB Sequence				
BB9	2.0	20.1	90.1	Strongly lateritized
BB8	5.0	6.4	67.7	Moderately lateritized
BB7	6.0	52.8	61.7	Weakly lateritized
BB6*	11.0	2.9	93.8	Strongly lateritized
BB5	13.0	2.6	67.2	Allochthonous inputs
BB4*	15.0	1.8	58.0	Weakly lateritized
BB3	26.0	0.2	59.0	Weakly lateritized
BB2*	35.0	6.5	34.5	
BB1*	47.0		35.7	
	Total	93.2		
SQ Sequence				
SQ14	0.0	-0.8	85.8	Strongly lateritized
SQ13	2.5	-0.8	82.0	Strongly lateritized
SQ12	3.5	-0.9	79.8	Moderately lateritized
SQ11	7.5	1.3	84.3	Strongly lateritized
SQ10	8.5	-0.9	82.3	Strongly lateritized
SQ9	12.0	-0.9	30.5	Kaolinized
SQ8	13.5	-0.8	30.7	Kaolinized
SQ7	14.0	-0.8	26.9	Kaolinized
SQ6	15.0	-0.2	18.3	
SQ5	22.5	0.5	27.2	Kaolinized
SQ4	25.5	-0.2	14.8	
SQ3	30.0	-0.3	21.9	
SQ2	34.0		23.4	
	Total	-4.8		

τ- values calculated following Chadwick et al. (1990). The BB sequence is calculated relative to BB1 protolith values from Babechuk et al., 2014 (Supplementary Sheet 1). The Index of Lateritization is calculated following Schellman (1986), using major oxide wt% values from Widdowson (2007) alongside degrees of lateritization determined by Widdowson (2007) from ternary plots.

867

868 **FIGURE CAPTIONS**

869 Figure 1: Literature compilation of Tl concentrations and Tl stable isotopes ($\varepsilon^{205}Tl$) for
870 terrestrial and major marine sediments and reservoirs. (a – d) FeMn deposits (Rehkämper et
871 al., 2002), (e) mantle (Nielsen et al., 2006b), (f) low temperature altered ocean crust (Nielsen
872 et al., 2006a), (g – j) volcaniclastics/radiolarian and claystone/pelagic clays (Prytulak et al.,
873 2013 and Nielsen et al., 2017b), (j) diatom-bearing sediments (Nielsen et al., 2016), (k – l)
874 river water and loess averages (Nielsen et al., 2005), (m) continental crust average (Nielsen et
875 al., 2017a)., (n) soils (Kersten et al., 2014), and laterite values measured in this study. Where
876 average ranges specified $\varepsilon^{205}Tl \pm 1SD$ are reported.
877
878 Figure 2: Inset showing the study region and map of the location of the two laterite
879 sequences (adapted from Wimpenny et al., 2007).
880
881 Figure 3: Schematic profiles of the laterite sequences at a) Goa (SQ) and b) Bidar (BB),
882 alongside alteration zones (adapted from Wimpenny et al., 2007). Zone I = unaltered to
883 weakly altered substrate, II = saprolite, III = palaeowater table and IV = Fe-rich lateritic cap,
884 as noted by Widdowson (2007). Samples analysed in this study for trace element
885 concentrations highlighted in colour and for Tl stable isotopes denoted by an *. Values for
886 K_2O, MnO and MgO content plotted on log axes. Measured values denoted by filled symbols
887 and literature values by unfilled symbols throughout (Widdowson, 2007).
888
889 Figure 4: (a) Thallium concentration versus depth-for the SQ greywacke (orange
890 throughout) and BB basalt (blue throughout) – based laterites. (b) Thallium stable isotope
891 variations with depth for the greywacke and basalt. The deepest basaltic sample at 47 m
892 (BB1) is an estimated unaltered basaltic or mantle composition (Nielsen et al., 2017a).

Figure 5: Trace element data for alkali elements, alkaline earths and Tl for the a) SQ profile, measured in this study using ICP-QQQ. and b) BB profile, with both measured and literature values. Alkali elements and alkaline earth elements plotted on log scale and where used, literature values are denoted by unfilled symbols (see Supplementary Sheet 1; Widdowson, 2007 and Wimpenny et al., 2007).

Figure 6: Thallium concentrations and $\varepsilon^{205}Tl$ variations for the greywacke (orange) and basalt (blue). BB5 and SQ11 display heavy positive excursions. Literature values for BB1 denoted by unfilled triangle (Nielsen et al., 2017a).

Figure 7: $\tau_{Tl/Zr}$ variations with depth through the (a) SQ profile and (b) BB profile. Both profiles show contrasting behaviours in net trends but horizons with distinct Tl addition are present in both. For the BB profile literature values for Tl and Zr concentrations are denoted by unfilled symbols (see Supplementary Sheet 1, Widdowson (2007)).

Figure 8: The effect of increasing intensity of lateritization on Tl concentration. Zones are labelled, with Zone I = unaltered to weakly altered substrate, II = saprolite, III = palaeowater table and IV = Fe-rich lateritic cap throughout.

Figure 9: The role of increasing weathering intensity, as quantified by the index of lateritization, on Tl stable isotopes across the SQ profile. Correlation is shown for samples not weathered beyond the stage of kaolinization (Widdowson, 2007).

Figure 10: Trends within the SQ profile between $\varepsilon^{205}Tl$ and $\tau_{Tl/Zr}$ through the full profile (a) are masked by the large excursive palaeowater table horizon (SQ11, Zone III). Further analysis discounting SQ11 show a weak negative correlation between Tl stable isotope composition and Tl enrichments.

Figure 11: The effect of weathering on $\tau_{Tl/Zr}$ (as a measure of Tl mobility within the SQ profile).

SUPPLEMENTARY MATERIAL

Supplementary Sheet 1: Major elemental literature compilation from Widdowson, 2007.

Supplementary Sheet 2: Trace elemental literature compilation from Widdowson, 2007 and Babechuk et al., 2014.

Supplementary Sheet 3: Trace element data quality control.

Supplementary Sheet 4: Trace elemental data from ICP-QQQ.

Electronic Annex: Comparison of methods for determination of thallium Tl concentration using ICP-MS (Open University) and MC ICP-MS (Imperial College London).

TABLES

Table 1 Thallium concentrations and $\varepsilon^{205}Tl$ from MC-ICPMS (Imperial College London) and ICP-MS (Open University) analyses of the basaltic BB and greywacke SQ laterite sequences. A standard error of ±0.4 $\varepsilon^{205}Tl$ from long-term reproducibility is applied except in cases where this value is exceeded.

Sample	Depth (m)	Lithology	[Tl] ng/g MC-ICPMS	[Tl] ng/g ICP-MS	$\varepsilon^{205}Tl$	2sd	# runs	# dissolutions
SQ2	34.0	Unweathered greywacke	559	540	-2.3	0.4	5	1
SQ3	30.0	Lighter greywacke	459	444	-1.3	0.5	1	1
SQ4	25.5	Soft weathered greywacke	231	218	-2.4	0.6	2	1
SQ5	22.5	Weathered greywacke	700	652	-2.1	0.6	4	2
SQ6	15.0	Red weathered greywacke	340	324	-1.9	0.5	1	1
SQ7	14.0	Base of laterite	148	126	-1.1	0.5	7	4
SQ8	13.5	Nodular laterite base	76	105	-0.5	0.4	2	1
SQ9	12.0	Nodular laterite	95	81	+0.3	0.4	2	1
SQ10	8.5	Semi-indurated laterite	40	37	-1.2	0.4	2	1
SQ11	7.5	Massive laterite	456	544	+3.5	0.6	2	1
SQ12	3.5	Indurated laterite cap	103	105	-1.0	0.4	2	1
SQ13	2.5	Indurated laterite cap	127	135	-1.0	0.4	4	1
BB5: Average	13.0	Basaltic saprolite	24	26	+6.2	1.5	4	3
BB5: Separate Runs								
BB5-1			27		+5.3			
BB5-2			25		+5.9			
BB5-2			25		+6.4			
BB5-3			28		+7.1			
BB7	6.0	Base of laterite	252	244	+0.3	0.5	1	1
BB8	5.0	Nodular laterite	38	39	-0.5	0.4	3	2

Table 2 Thallium concentrations and $\varepsilon^{205}Tl$ of reference materials measured in this study from MC-ICPMS (Imperial College London) and ICP-MS (Open University) analyses and from literature.

Reference Materials		[Tl] ng/g MC-ICPMS	[Tl] ng/g ICP-MS	$\varepsilon^{205}Tl$	2sd	# runs	# dissolutions
AGV-2, This study	Andesitic USGS standard	222		-2.6	0.6	10	4
AGV-2, Nielsen et al., 2017a	Andesitic USGS standard	269		-3.0	0.6	8	8
BCR-2, This study	Basaltic USGS standard	255		-2.5	0.4	4	2
BCR-2, Nielsen et al., 2017a	Basaltic USGS standard	257		-2.5	0.4	4	4
VL2	Venezuelan laterite standard	29	30	+2.1	0.5	2	2

Table 3 Trace element concentrations determined by ICP-MS at the Open University (μg/g).

	BB3	BB5	BB7	BB8	SQ1	SQ2	SQ3	SQ4	SQ5	SQ6	SQ7	SQ8	SQ9	SQ10	SQ11	SQ12	SQ13	SQ14	VL1	VL2
Li	6.8	3.7	11.2	17.4	7.4	31.6	32.4	12.5	45.0	20.2	13.8	9.7	8.7	4.5	4.2	7.1	9.5	8.8	0.1	2.8
Sc	68	77	34	47	43	12	13	7	11	10	15	16	17	24	27	28	38	66	64	82
Ti	26903	29298	16215	11650	8522	3243	3391	1809	2922	2563	4129	4558	3836	8646	2857	10307	8624	9471	16771	15681
V	730	1997	704	992	366	99	102	56	94	84	121	143	138	852	112	578	822	788	775	587
Cr	206	261	228	744	115	109	118	63	79	83	87	112	125	720	166	720	946	749	98	25
Mn	775	395	2401	464	1941	1031	831	508	1404	413	429	162	99	130	3720	344	256	245	494	730
Co	67	14	40	18	63	19	19	6	20	10	11	3	3	3	38	8	5	6	7	38
Ni	305	73	63	102	90	42	47	15	41	23	69	42	38	69	147	58	59	58	6	37
Cu	446	519	228	196	122	50	40	66	37	53	42	38	34	31	52	39	50	61	105	255
Zn	126	72	62	74	127	112	115	33	146	66	38	38	23	21	97	25	25	31	60	99
Rb	1.24	0.83	1.57	4.12	18.32	126.77	108.53	46.57	147.69	79.03	40.83	31.17	26.86	9.02	16.31	22.07	28.07	27.59	0.37	1.37
Sr	14	6	16	10	243	117	113	104	86	113	7	9	7	21	40	40	35	41	1	1
Y	796	14	6	8	31	17	27	13	17	40	12	9	8	10	27	17	14	19	3	7
Zr	253	315	193	224	66	172	192	83	137	123	213	196	191	203	76	261	217	236	421	419
Nb	19.6	25.5	15.2	17.0	3.3	13.8	15.0	7.1	12.5	10.8	16.8	17.6	16.0	20.8	8.1	32.9	27.3	30.7	17.2	18.2
Sb	0.09	0.31	0.81	1.41	0.02	0.24	0.34	0.24	0.30	0.26	0.41	0.62	0.60	11.53	1.12	8.40	14.46	8.30	0.74	0.31
Cs	0.112	0.101	0.140	0.403	0.556	4.314	3.538	1.284	4.506	2.104	1.107	1.502	0.896	0.441	1.704	1.323	1.920	1.595	0.011	0.092
Ba	57	16	445	18	144	702	609	404	665	549	571	473	454	46	730	136	136	125	6	32
La	33.3	9.6	28.7	13.3	8.2	25.7	41.9	15.1	13.4	72.1	7.3	6.9	3.4	19.6	54.0	40.6	29.4	32.1	2.1	4.4
Ce	25.9	22.5	270.1	27.6	20.4	52.8	75.5	32.7	27.8	98.9	63.4	21.2	9.1	33.5	87.9	87.3	63.1	60.1	14.7	164.4
Pr	16.78	4.07	3.97	2.61	2.85	5.62	7.88	3.50	2.96	12.38	1.99	1.64	0.81	2.97	8.49	6.33	4.90	5.66	0.47	1.29
Nd	77.3	18.2	11.9	9.5	13.7	20.1	28.1	12.7	10.7	43.4	7.6	6.0	3.1	9.4	26.5	20.1	16.0	19.4	1.8	5.4
Sm	29.70	4.49	2.01	1.98	3.85	3.72	5.06	2.51	2.14	7.91	1.58	1.18	0.68	1.55	4.93	3.23	2.78	3.51	0.53	1.59
Eu	12.27	1.11	0.51	0.48	1.41	0.82	0.96	0.57	0.54	1.62	0.40	0.31	0.22	0.31	1.14	0.58	0.53	0.67	0.15	0.42
Gd	56.98	3.62	2.64	1.72	4.28	3.02	4.41	2.27	1.98	7.45	1.53	1.02	0.64	1.33	5.11	2.64	2.29	2.87	0.51	1.91
Tb	12.85	0.63	0.28	0.30	0.77	0.46	0.67	0.36	0.33	1.14	0.25	0.18	0.13	0.22	0.82	0.40	0.37	0.46	0.11	0.27
Dy	93.32	3.65	1.50	1.85	4.93	2.67	3.95	2.18	2.13	6.36	1.74	1.29	1.00	1.47	4.94	2.53	2.31	3.06	0.73	1.69
Ho	24.79	0.76	0.32	0.42	1.11	0.59	0.87	0.46	0.53	1.28	0.42	0.33	0.27	0.35	1.07	0.61	0.53	0.67	0.18	0.38
Er	64.05	1.97	0.84	1.14	3.07	1.84	2.59	1.32	1.77	3.40	1.42	1.11	0.94	1.13	2.96	1.87	1.68	2.04	0.55	1.13
Yb	53.87	1.99	0.90	1.27	2.89	2.23	2.75	1.32	2.24	2.97	1.95	1.59	1.44	1.47	2.98	2.26	1.95	2.37	0.77	1.54
Hf	7.03	8.47	5.20	5.73	1.82	4.63	5.09	2.29	3.65	3.22	5.67	5.22	5.21	5.48	2.10	7.05	5.82	6.16	11.73	11.32
Lu	8.29	0.30	0.14	0.20	0.45	0.35	0.42	0.20	0.40	0.42	0.32	0.28	0.25	0.22	0.46	0.37	0.31	0.38	0.13	0.25
Ta	1.44	1.72	1.53	1.16	0.19	1.36	1.45	0.61	1.03	1.06	1.73	1.64	1.53	1.48	0.62	3.08	1.78	2.30	1.14	1.18
Tl	0.007	0.026	0.244	0.039	0.075	0.540	0.444	0.218	0.652	0.324	0.126	0.105	0.081	0.037	0.544	0.105	0.135	0.129	0.006	0.030
Pb	2.30	10.43	46.46	19.19	2.77	12.85	12.75	11.62	13.97	10.78	28.09	17.68	15.26	31.24	29.10	54.60	42.17	35.84	7.99	39.02
Th	1.92	3.60	3.82	10.06	0.47	21.06	21.51	7.61	15.51	13.63	26.82	21.94	23.64	20.80	6.06	24.91	22.02	22.61	14.00	11.02
U	1.01	2.19	1.24	2.00	0.09	5.90	6.32	2.19	4.81	4.07	6.29	5.81	6.21	4.52	6.79	6.65	7.39	10.37	1.69	3.14
Sn	1.85	0.53	0.79	1.09	0.75	3.11	2.34	1.71	3.84	1.98	3.25	3.20	3.09	2.61	1.45	5.46	2.69	3.01	2.47	0.46

Table 4 τ-values and Index of lateritization (IOL) values for BB and SQ profiles.

Sample	Depth (m)	τ-value	IOL	Degree of lateritization (Widdowson 2007)
BB Sequence				
BB9	2.0	20.1	90.1	Strongly lateritized
BB8	5.0	6.4	67.7	Moderately lateritized
BB7	6.0	52.8	61.7	Weakly lateritized
BB6*	11.0	2.9	93.8	Strongly lateritized
BB5	13.0	2.6	67.2	Allochthonous inputs
BB4*	15.0	1.8	58.0	Weakly lateritized
BB3	26.0	0.2	59.0	Weakly lateritized
BB2*	35.0	6.5	34.5	
BB1*	47.0		35.7	
	Total	93.2		
SQ Sequence				
SQ14	0.0	-0.8	85.8	Strongly lateritized
SQ13	2.5	-0.8	82.0	Strongly lateritized
SQ12	3.5	-0.9	79.8	Moderately lateritized
SQ11	7.5	1.3	84.3	Strongly lateritized
SQ10	8.5	-0.9	82.3	Strongly lateritized
SQ9	12.0	-0.9	30.5	Kaolinized
SQ8	13.5	-0.8	30.7	Kaolinized
SQ7	14.0	-0.8	26.9	Kaolinized
SQ6	15.0	-0.2	18.3	
SQ5	22.5	0.5	27.2	Kaolinized
SQ4	25.5	-0.2	14.8	
SQ3	30.0	-0.3	21.9	
SQ2	34.0		23.4	
	Total	-4.8		

τ- values calculated following Chadwick et al. (1990). The BB sequence is calculated relative to BB1 protolith values from Babechuk et al., 2014 (Supplementary Sheet 1). The Index of Lateritization is calculated following Schellman (1986), using major oxide wt% values from Widdowson (2007) alongside degrees of lateritization determined by Widdowson (2007) from ternary plots.

Figure 1

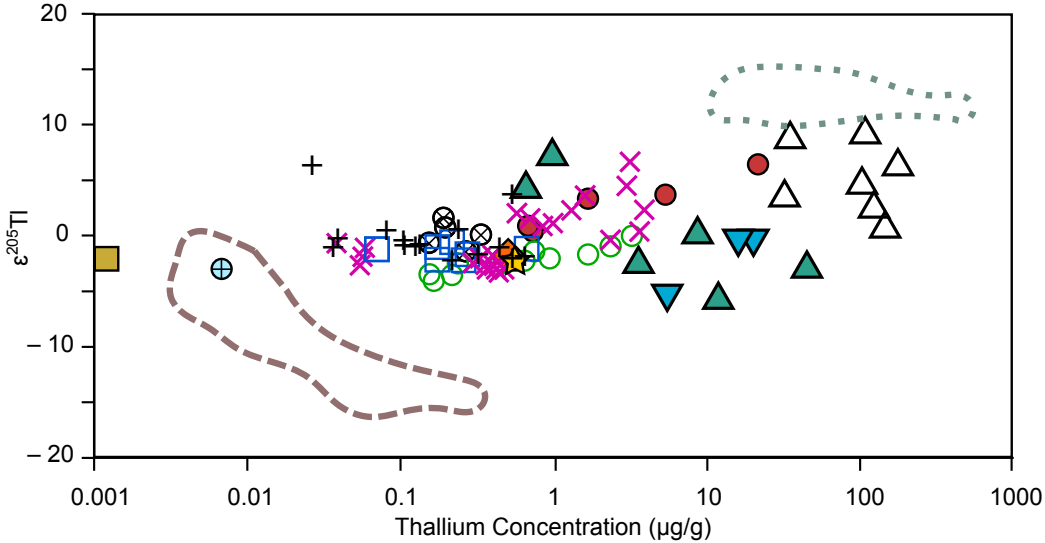

Hydrogenetic FeMn deposits[a]
Hydrothermal FeMn deposits[b]
Shallow water diagenetic FeMn deposits[c]
Deep water diagenetic FeMn deposits[d]
Mantle[e]
Low-T altered oceanic crust[f]
Red-brown clays[g]
Pelagic clays and silts[h]
Volcaniclastics[i]
Diatom-bearing sediments[j]
River water average ± 1.9[k]
Loess average ± 0.3[l]
Continental crust average ± 1[m]
Soils[n]
Laterites (this study)

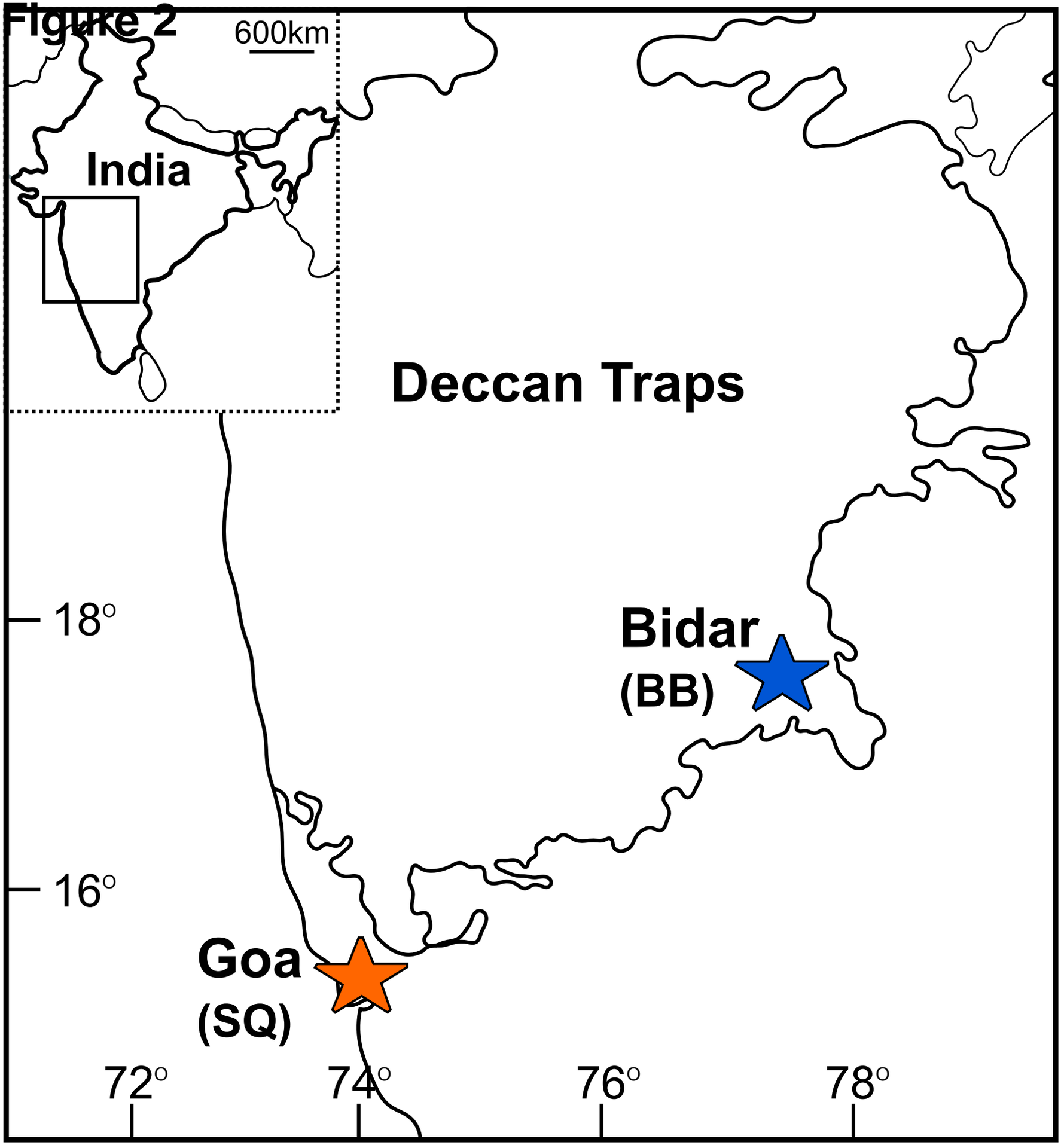
Figure 2
600km
India
Deccan Traps
18°
16°
Bidar
(BB)
Goa
(SQ)
72°
74°
76°
78°

Figure 3

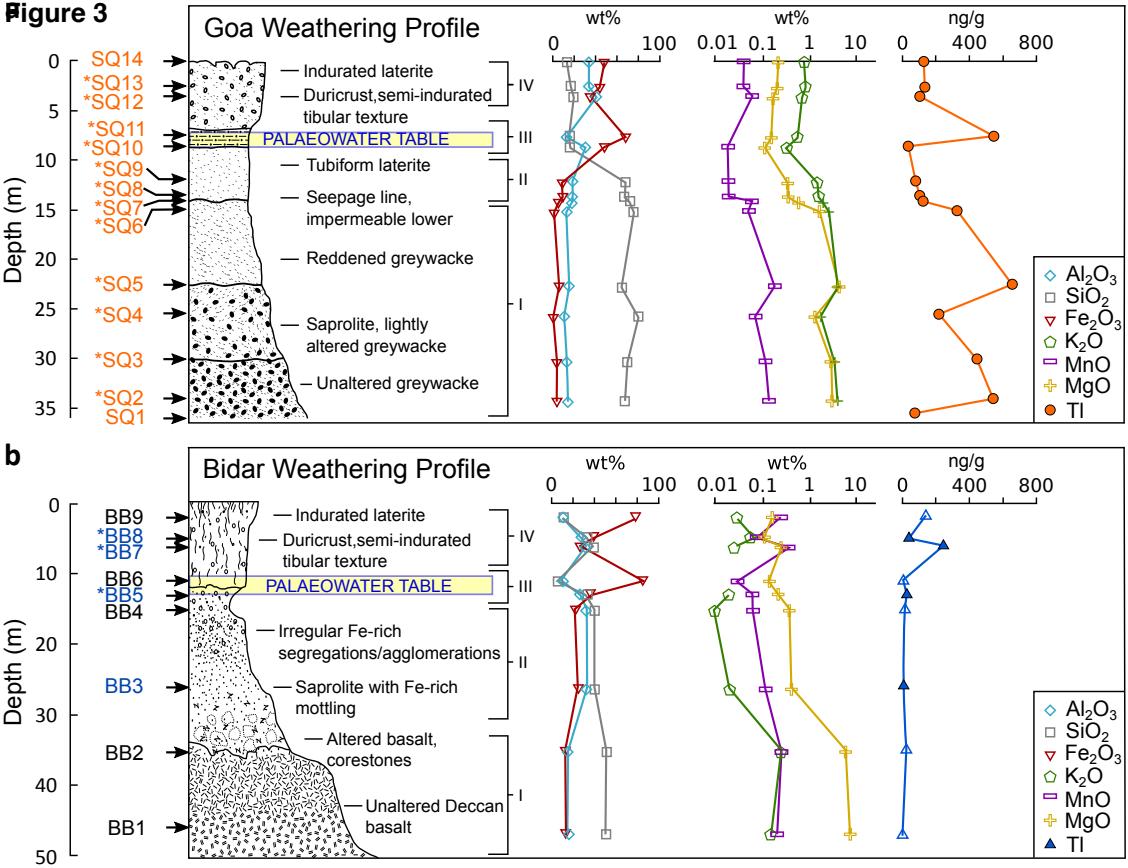
a
Goa Weathering Profile
wt%
wt%
ng/g
Depth (m)
SQ14
*SQ13
*SQ12
*SQ11
*SQ10
*SQ9
*SQ8
*SQ7
*SQ6
*SQ5
*SQ4
*SQ3
*SQ2
SQ1
Indurated laterite
Duricrust,semi-indurated tibular texture
PALAEOWATER TABLE
Tubiform laterite
Seepage line, impermeable lower
Reddened greywacke
Saprolite, lightly altered greywacke
Unaltered greywacke
IV
III
II
I
Al2O3
SiO2
Fe2O3
K2O
MnO
MgO
Tl
b
Bidar Weathering Profile
wt%
wt%
ng/g
Depth (m)
BB9
*BB8
*BB7
BB6
*BB5
BB4
BB3
BB2
BB1
Indurated laterite
Duricrust,semi-indurated tibular texture
PALAEOWATER TABLE
Irregular Fe-rich segregations/agglomerations
Saprolite with Fe-rich mottling
Altered basalt, corestones
Unaltered Deccan basalt
IV
III
II
I
Al2O3
SiO2
Fe2O3
K2O
MnO
MgO
Tl

Figure 4

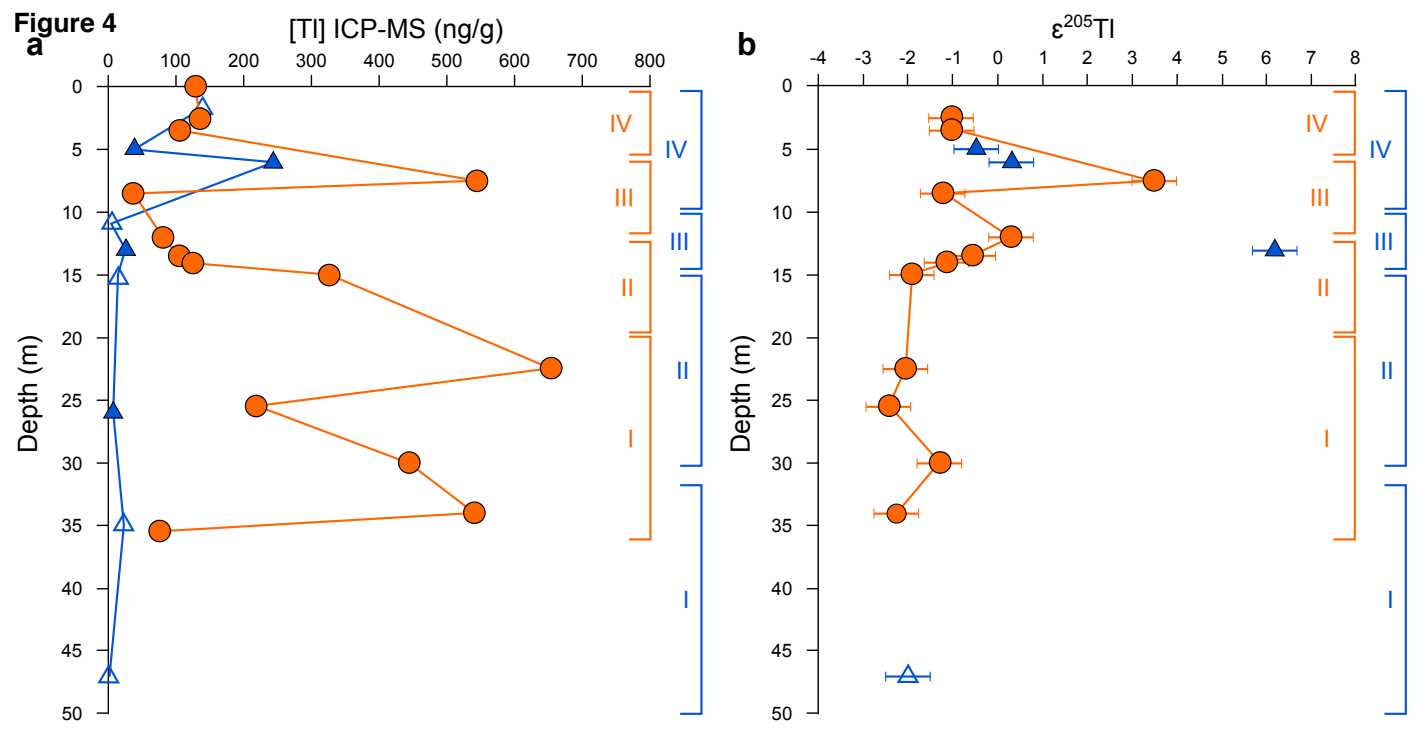
a
[Tl] ICP-MS (ng/g)
0
100
200
300
400
500
600
700
800
Depth (m)
0
5
10
15
20
25
30
35
40
45
50
IV
III
II
I
b
ε205Tl
-4
-3
-2
-1
0
1
2
3
4
5
6
7
8

Figure 5

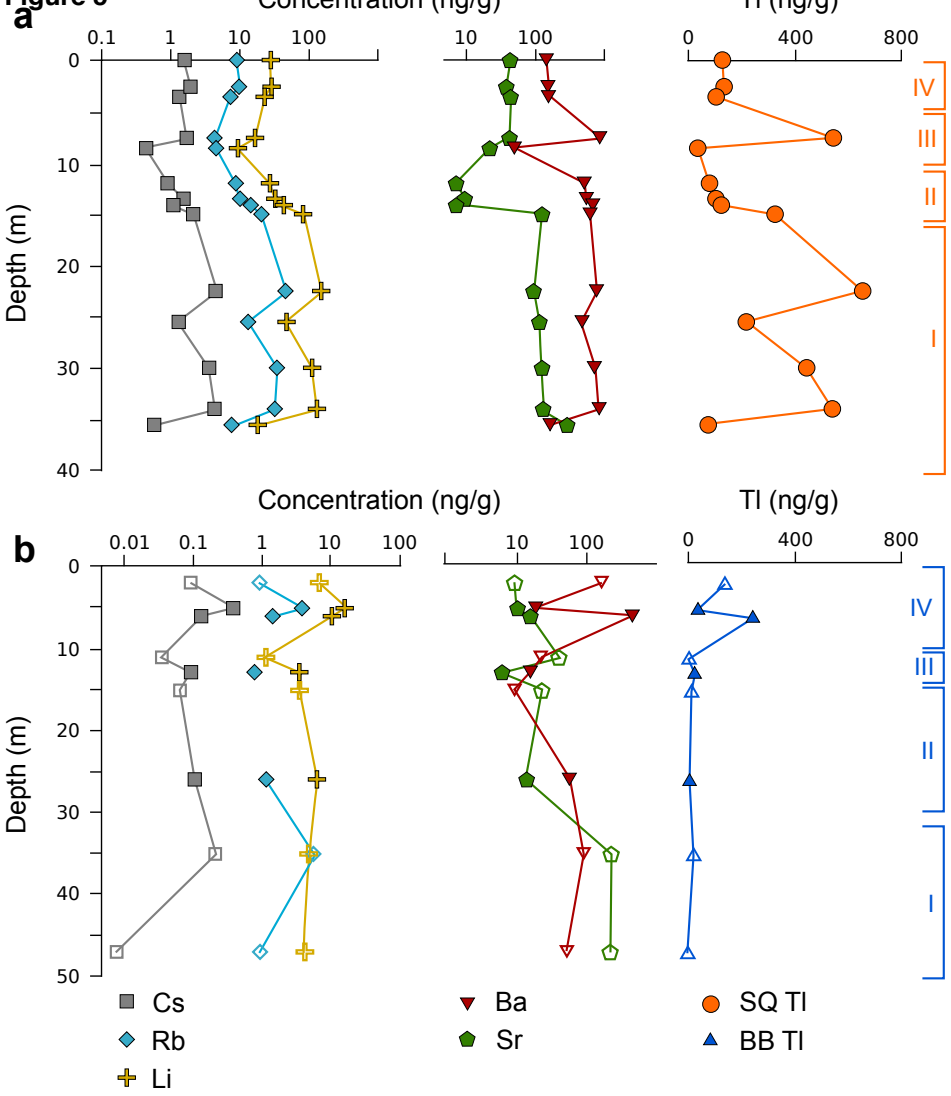
a
Concentration (ng/g)
0.1
1
10
100
10
100
Tl (ng/g)
0
400
800
Depth (m)
0
10
20
30
40
IV
III
II
I
b
Concentration (ng/g)
0.01
0.1
1
10
100
10
100
Tl (ng/g)
0
400
800
Depth (m)
0
10
20
30
40
50
IV
III
II
I
Cs
Rb
Li
Ba
Sr
SQ Tl
BB Tl

Figure 6

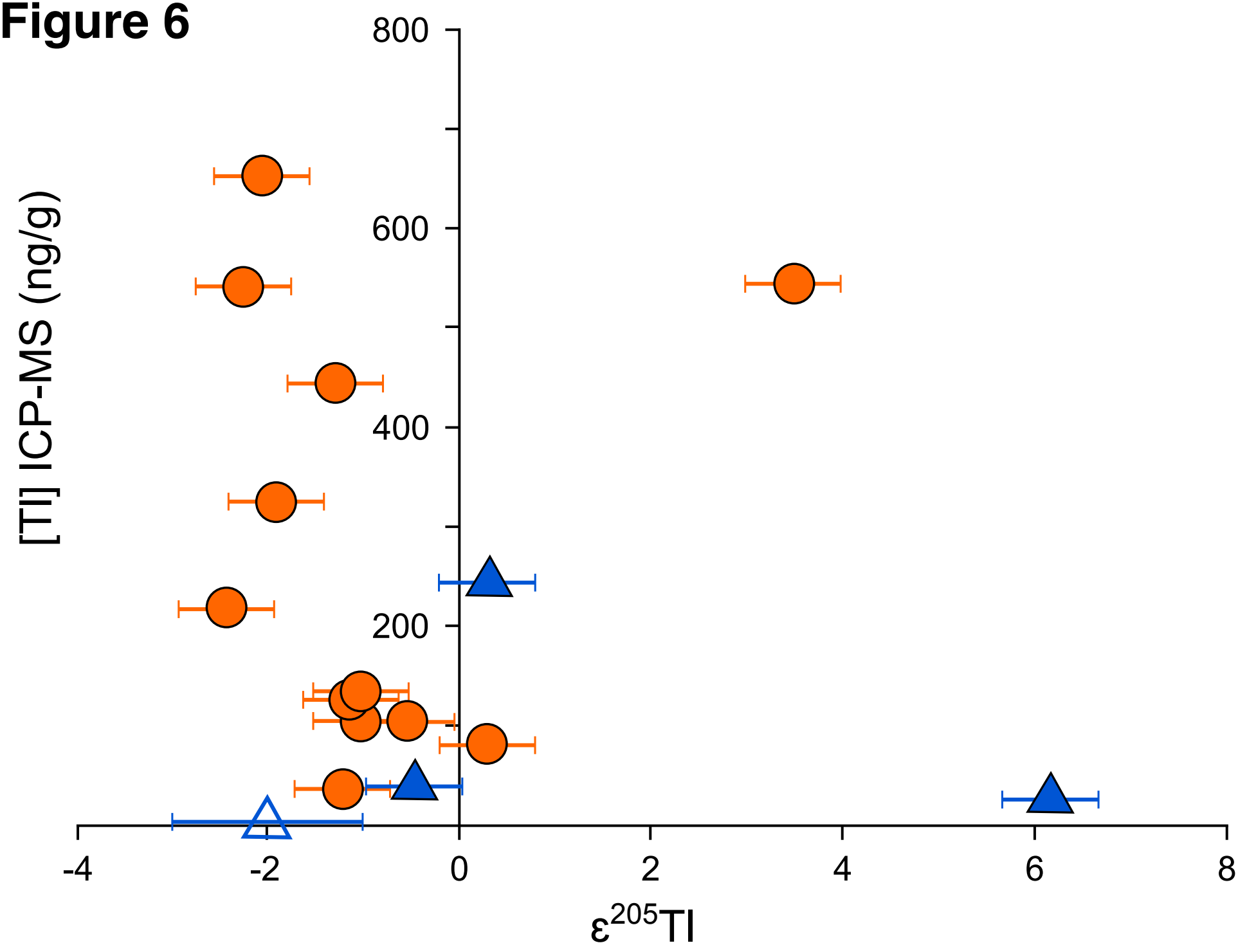

Figure 7

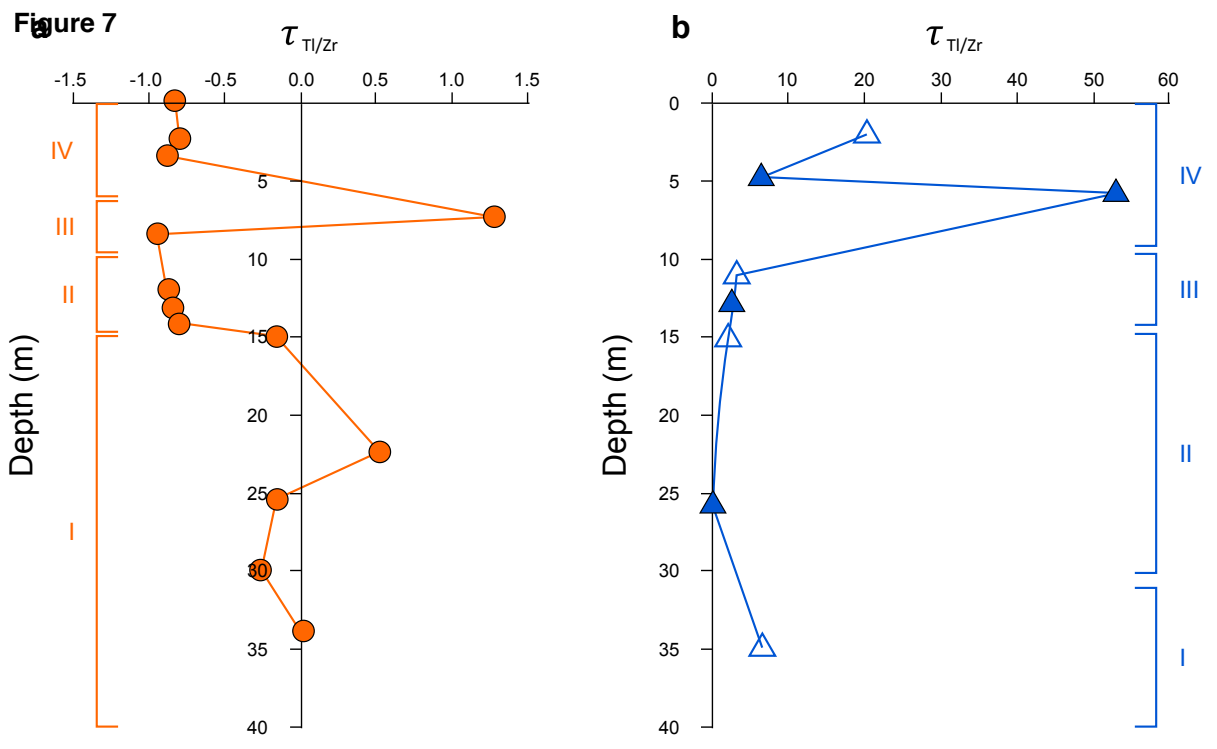
a
b
$\tau_{Tl/Zr}$
Depth (m)
IV
III
II
I
-1.5
-1.0
-0.5
0.0
0.5
1.0
1.5
0
10
20
30
40
50
60
5
15
25
35

Figure 8

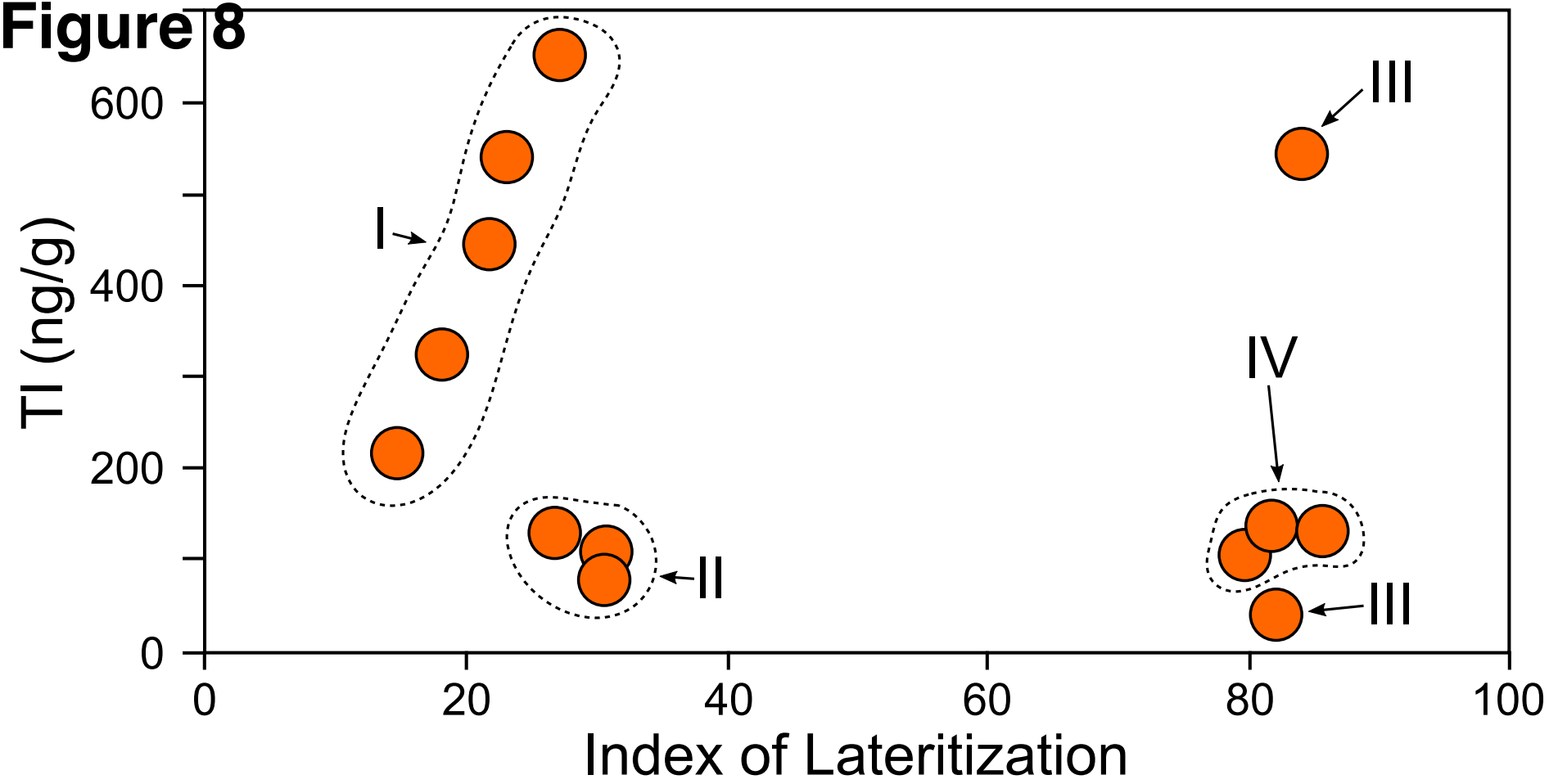
600
400
200
0
TI (ng/g)
0
20
40
60
80
100
Index of Lateritization
I
II
III
IV
III

Figure 9

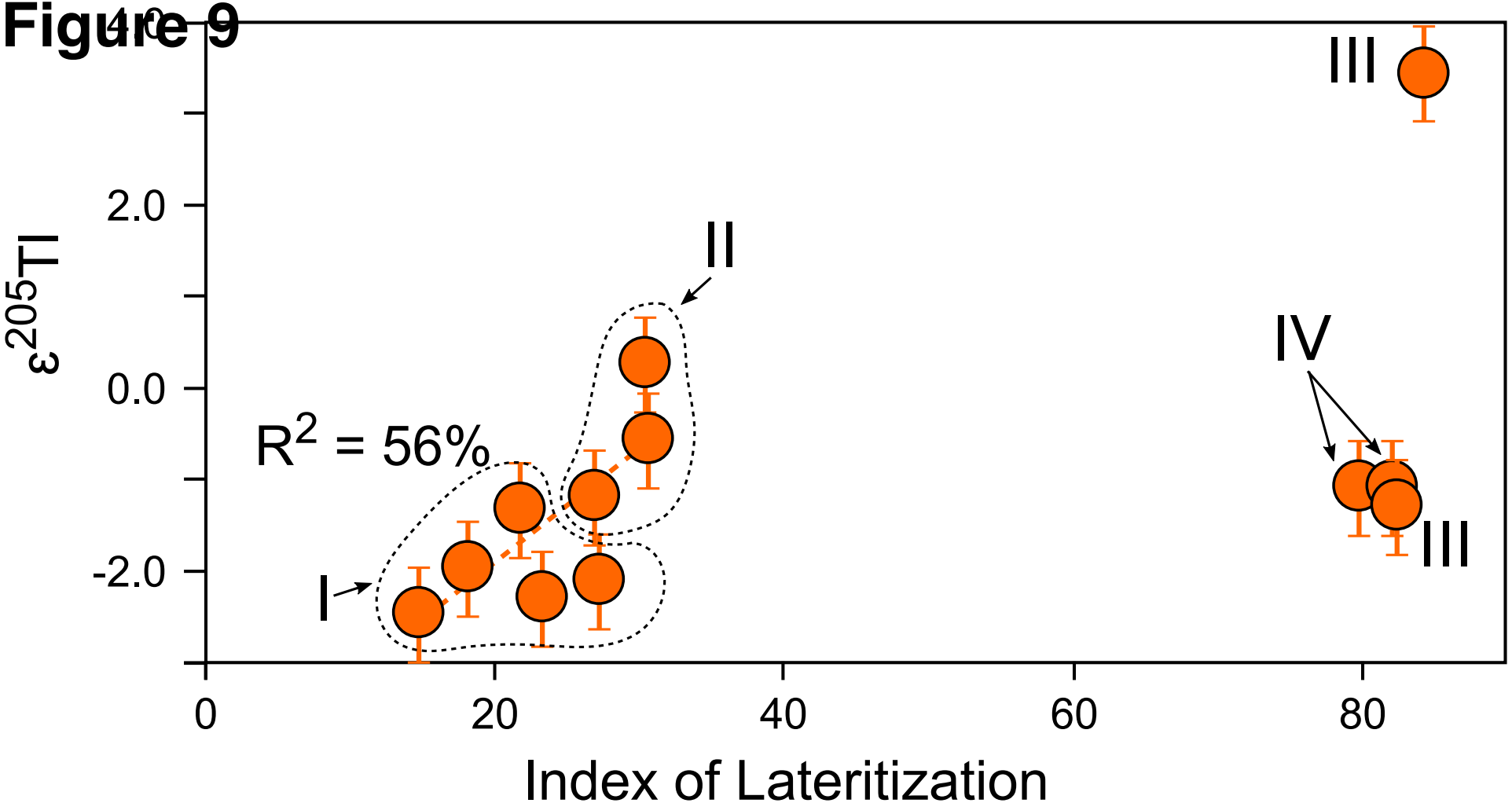
4.0
2.0
0.0
-2.0
ε^{205}Tl
0
20
40
60
80
Index of Lateritization
R^2 = 56%
I
II
III
IV
III

Figure 10

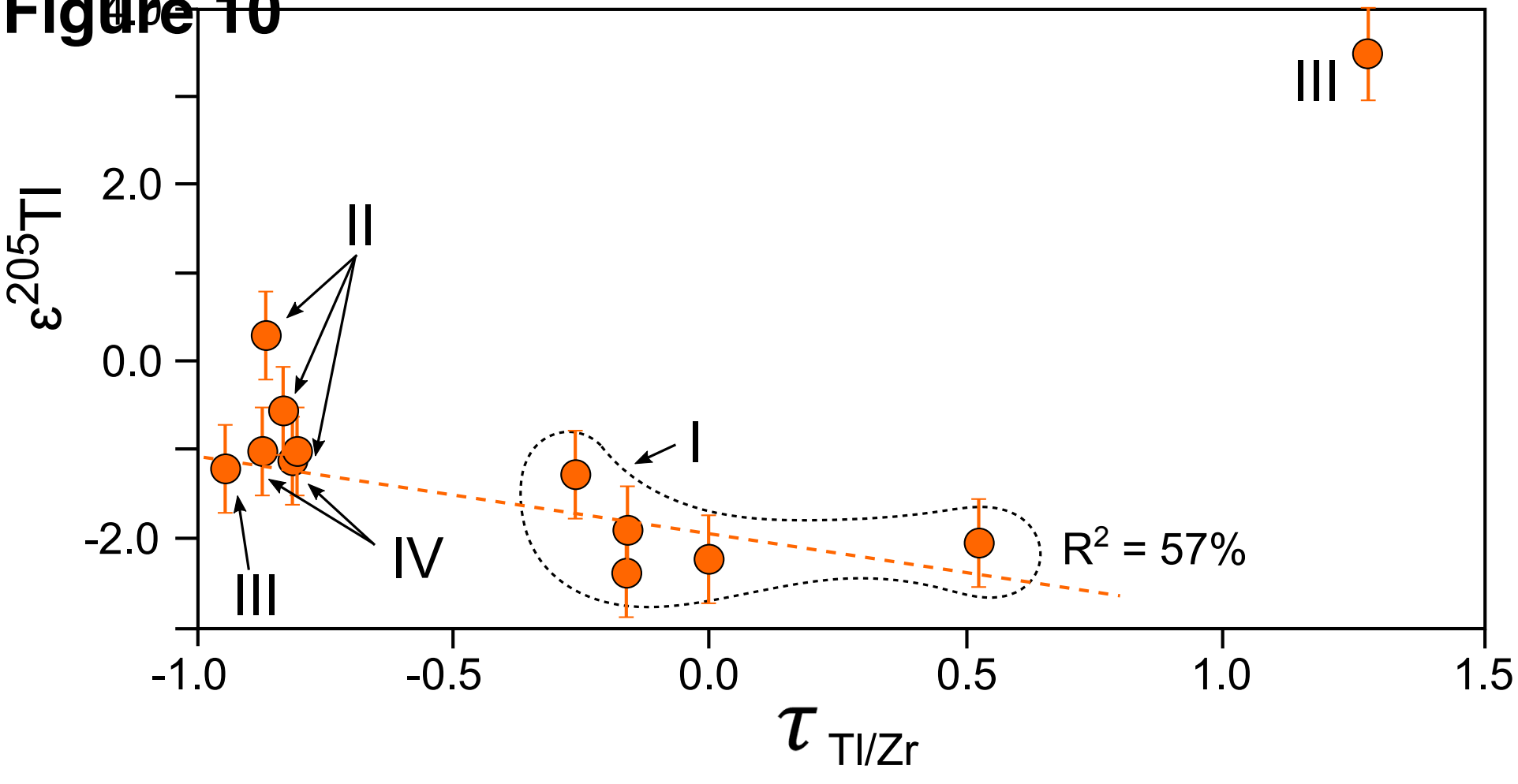
III
II
I
IV
III
R^2 = 57%
ε^{205}Tl
2.0
0.0
-2.0
-1.0
-0.5
0.0
0.5
1.0
1.5
$\tau_{Tl/Zr}$

Figure 11

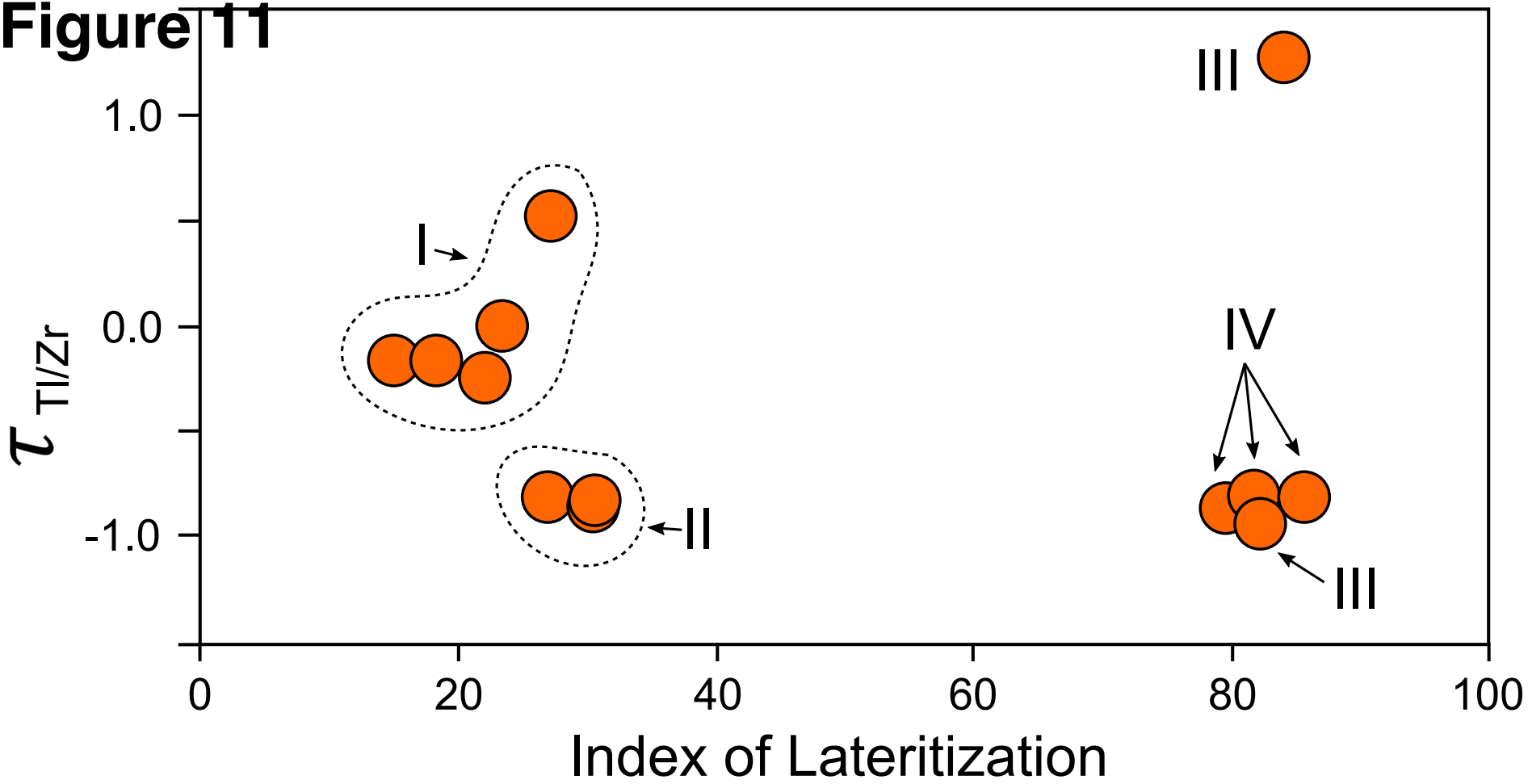
1.0
0.0
-1.0
τ Tl/Zr
0
20
40
60
80
100
Index of Lateritization
I
II
III
IV
III

Supplementary Sheet

Click here to download Appendix: Supplementary Sheet.xls

Formulae

Click here to download Appendix: FORMULAE.pdf

Electronic Annex Figure

Click here to download Electronic Annex: ElectronicAnnexFigure.pdf